Self-consistent theory of vortex dynamics in disordered superconductors

Staffan Grundberg and Jørgen Rammer
Department of Theoretical Physics, Umeå University, S-901 87 Umeå, Sweden
(Received 10 June 1999)

The influence of pinning on vortex dynamics in type-II superconductors is investigated. The vortex dynamics is described by the Langevin equation, and a field-theoretic formulation of the pinning problem allows the average over the quenched disorder to be performed exactly. A self-consistent theory is constructed using the diagrammatic functional method for the effective action, allowing a determination of the vortex response to external forces, the vortex fluctuations, and the pinning of vortices due to quenched disorder. The dependence of the pinning force on vortex velocity, temperature, and disorder strength is calculated for independent vortices as well as for a vortex lattice, and both analytical and numerical results for the pinning of vortices in the flux flow regime are obtained. The validity of the self-consistent theory is ascertained by comparing with numerical simulations of the Langevin equation. Furthermore, the influence of a Hall force on the pinning force is considered. Finally, the influence of pinning on the dynamic melting of a vortex lattice is studied.

I. INTRODUCTION

The advent of high-temperature superconductors has led to a renewed interest in vortex dynamics, since high-temperature superconductors have large values of the Ginzburg-Landau parameter and the HT-phase diagram is dominated by the vortex phase. At intermediate values of the magnetic field, i.e., between H_{c1} and H_{c2}, the magnetic flux will penetrate a type-II superconductor in the form of flux tubes, each carrying the quantized magnetic flux $\phi_0 = h/2e$, corresponding to vortex lines in the superconducting order parameter. The pinning of vortices due to defects, e.g., twin boundaries and impurities, is of importance for technological applications of superconductors, since a supercurrent in a perfect superconductor will lead to motion of the vortex lattice, resulting in dissipation. In this paper we report a detailed study of the influence of quenched disorder on the vortex dynamics in type-II superconductors in the flux flow regime.

In recent years a large number of papers studying vortex pinning experimentally as well as theoretically have appeared. Examples of the considered topics are pinning of vortex liquids,[1] depinning of flux lines,[2] and the interference effect between an external ac current and the intrinsic oscillations of the vortex lattice.[3] Special interest has been paid to the subject of dynamic melting of the vortex lattice, and a number of experimental works have been reported.[4] Several simulations of dynamic melting have also been reported[5] following the original work on dynamic melting.[6]

Vortex pinning in the flux flow regime was originally considered by Schmid and Hauger[7] and Larkin and Ovchinnikov.[8] In these works, the disorder was treated in lowest-order perturbation theory. Later, Müllers and Schmid[9] applied the field-theoretical method of Cornwall, Jackiw, and Tomboulis[10] to the pinning of vortices. The field-theoretical method will be used in the present work, and extended to discuss the influence of a Hall force and dynamic melting of the vortex lattice. Furthermore, we have performed numerical simulations that allow a quantitative assessment of the validity of the self-consistent theory of vortex pinning.

The cases of interacting as well as noninteracting vortices are considered, the latter case being appropriate for low magnetic fields, where the vortices are so widely separated that the interaction between them can be neglected. The self-consistent theory is compared to numerical simulations of the dynamics of a single vortex, as well as with analytical results obtained in limiting cases. The influence of a Hall force on the pinning of a single vortex is also studied, and we find that its effect is qualitatively different depending on the magnitude of the temperature. For the case of interacting vortices forming a vortex lattice, the dependence of the pinning force on velocity, temperature, and stiffness of the lattice is calculated. We then consider how the pinning of a vortex lattice is influenced by a Hall force. Finally, we consider the dynamic melting transition of a vortex lattice. We calculate the relative vortex displacement fluctuations as a function of velocity, and by employing a modified Lindemann criterion, we determine the velocity dependence of the melting temperature. We obtain the phase diagram for dynamic melting, and find that in contrast to perturbation theory, the melting curve evaluated numerically from the self-consistent theory is in quantitative agreement with simulations and experimental data.

The paper is organized as follows. The model used to describe the vortex dynamics is presented in Sec. II. In Sec. III we present the field-theoretic formulation of the pinning problem, and construct a self-consistent theory. The case of a single vortex is studied in Sec. IV, and in Sec. V we study the pinning properties of a vortex lattice. In Sec. VI we consider the dynamic melting of a vortex lattice. Finally, in Sec. VII we summarize and conclude.

II. MODEL

We consider a two-dimensional (2D) description of the vortices, since we have a thin superconducting film or a 3D layered superconductor with uncorrelated disorder between the layers in mind. We shall be interested in the influence of quenched disorder on the vortex dynamics in the flux flow

regime. The description of the vortex dynamics will be based on the Langevin equation[11]

$$m\ddot{\mathbf{u}}_{\mathbf{R}t}+\eta\dot{\mathbf{u}}_{\mathbf{R}t}+\sum_{\mathbf{R}'}\Phi_{\mathbf{R}\mathbf{R}'}\mathbf{u}_{\mathbf{R}'t}$$
$$=\mathbf{F}+\alpha\dot{\mathbf{u}}_{\mathbf{R}t}\times\hat{\mathbf{z}}-\nabla V(\mathbf{R}+\mathbf{u}_{\mathbf{R}t})+\boldsymbol{\xi}_{\mathbf{R}t}, \quad (1)$$

where $\mathbf{u}_{\mathbf{R}t}$ is the displacement, normal to $\hat{\mathbf{z}}$, at time t of the vortex, which initially has equilibrium position $\mathbf{R}$, η is the friction coefficient, and m is a possible mass of the vortex (both per unit length). The interaction between the vortices is treated in the harmonic approximation and described by the dynamic matrix $\Phi_{\mathbf{R}\mathbf{R}'}$. The force (per unit length) on the right side of Eq. (1) consists of the Lorentz force, $\mathbf{F}=\phi_0\mathbf{j}\times\hat{\mathbf{z}}$, due to the transport current density $\mathbf{j}$, which we eventually assume constant; the second term on the right side is a possible Hall force, characterized by the parameter α, and V is the pinning potential due to the quenched disorder. The pinning is described by a Gaussian-distributed stochastic potential with zero mean, $\langle V(\mathbf{x})\rangle=0$, and thus characterized by its correlation function

$$\nu(\mathbf{x}-\mathbf{x}')=\langle V(\mathbf{x})V(\mathbf{x}')\rangle. \quad (2)$$

The thermal noise $\boldsymbol{\xi}$ is the white noise stochastic process with zero mean and correlation function specified according to the fluctuation-dissipation theorem (where now the brackets denote averaging with respect to the thermal noise)

$$\langle\xi^{\alpha}_{\mathbf{R}t}\xi^{\alpha'}_{\mathbf{R}'t'}\rangle=2\eta T\delta(t-t')\delta_{\mathbf{R}\mathbf{R}'}\delta_{\alpha\alpha'}, \quad (3)$$

and, since the forces are per unit length, the ''temperature'' T has the dimension of energy per unit length.

Upon averaging with respect to the thermal noise and the quenched disorder, the average restoring force of the lattice vanishes,

$$-\sum_{\mathbf{R}'}\Phi_{\mathbf{R}\mathbf{R}'}\langle\langle\mathbf{u}_{\mathbf{R}'t}\rangle\rangle=\mathbf{0}, \quad (4)$$

since the average displacement is the same for all vortices, and a rigid translation of the vortex lattice does not change its elastic energy, leaving the dynamic matrix with the symmetry property

$$\sum_{\mathbf{R}'}\Phi_{\mathbf{R}\mathbf{R}'}=\mathbf{0}. \quad (5)$$

Corresponding to the lattice reaching a constant steady-state velocity $\mathbf{v}=\langle\langle\dot{\mathbf{u}}_{\mathbf{R}t}\rangle\rangle$, the average force on any vortex vanishes:

$$\mathbf{F}+\mathbf{F}_f+\mathbf{F}_H+\mathbf{F}_p=\mathbf{0}; \quad (6)$$

i.e., there will be a balance between the Lorentz force $\mathbf{F}$, the average friction force $\mathbf{F}_f=-\eta\mathbf{v}$, the average Hall force $\mathbf{F}_H=\alpha\mathbf{v}\times\hat{\mathbf{z}}$, and the pinning force

$$\mathbf{F}_p=-\langle\langle\nabla V(\mathbf{R}+\mathbf{u}_{\mathbf{R}t})\rangle\rangle. \quad (7)$$

The pinning force is determined by the relative positions of the vortices with respect to the pinning centers and is invariant with respect to the change of the sign of α. The average velocity is the only vector characterizing the vortex motion which is invariant with respect to the change of the sign of α, and the pinning force is therefore antiparallel to the velocity.[12] Thus, the pinning yields a renormalization of the friction coefficient

$$-\eta\mathbf{v}+\mathbf{F}_p=-\eta_{\mathrm{eff}}\mathbf{v}. \quad (8)$$

The effective friction coefficient depends on the average velocity of the lattice, the disorder, the temperature, the interaction between the vortices, the Hall force, and a possible mass of the vortex. In the absence of disorder, the effective friction coefficient reduces to the bare friction coefficient η.

In the analytical and numerical calculations, the correlator of the pinning potential shall be taken as a Gaussian function with range r_p and strength ν_0:

$$\nu(\mathbf{x}-\mathbf{x}')=\frac{\nu_0}{2\pi r_p^2}e^{-(\mathbf{x}-\mathbf{x}')^2/2r_p^2}, \quad \nu(\mathbf{k})=\nu_0 e^{-r_p^2k^2}. \quad (9)$$

III. FIELD THEORY OF PINNING

The average vortex motion is conveniently described by reformulating the stochastic problem in terms of the field theory of classical statistical dynamics.[13] The probability functional for a realization $\{\mathbf{u}_{\mathbf{R}t}\}_{\mathbf{R}}$ of the motion of the vortex lattice is expressed as a functional integral over a set of auxiliary variables $\{\tilde{\mathbf{u}}_{\mathbf{R}t}\}_{\mathbf{R}}$, and we are led to consider the generating functional

$$\mathcal{Z}[\mathbf{F},\mathbf{J}]=\int\prod_{\mathbf{R}}\mathcal{D}\mathbf{u}_{\mathbf{R}t}\int\prod_{\mathbf{R}}\mathcal{D}\tilde{\mathbf{u}}_{\mathbf{R}t}\mathcal{J}e^{iS[\mathbf{u},\tilde{\mathbf{u}}]}, \quad (10)$$

where in the action

$$S[\mathbf{u},\tilde{\mathbf{u}}]=\tilde{\mathbf{u}}(D_R^{-1}\mathbf{u}+\mathbf{F}-\nabla V+\boldsymbol{\xi})+\mathbf{J}\mathbf{u} \quad (11)$$

the inverse free retarded Green's function is specified by

$$-D_R^{-1}\mathbf{u}_{\mathbf{R}t}=m\ddot{\mathbf{u}}_{\mathbf{R}t}+\eta\dot{\mathbf{u}}_{\mathbf{R}t}+\sum_{\mathbf{R}'}\Phi_{\mathbf{R}\mathbf{R}'}\mathbf{u}_{\mathbf{R}'t}+\alpha\hat{\mathbf{z}}\times\dot{\mathbf{u}}_{\mathbf{R}t}, \quad (12)$$

i.e.,

$$D_R^{-1}(\mathbf{R},t;\mathbf{R}',t')$$
$$=-\Phi_{\mathbf{R}\mathbf{R}'}\delta(t-t')-[(m\partial_t^2+\eta\partial_t)1-i\alpha\sigma^y\partial_t]$$
$$\times\delta_{\mathbf{R},\mathbf{R}'}\delta(t-t'), \quad (13)$$

where matrix notation is used for its Cartesian components; i.e., 1 and σ^y denote the unit matrix (occasionally suppressed for convenience) and the Pauli matrix in Cartesian space, respectively. The Fourier transform of the inverse free retarded Green's function is therefore the 2×2 matrix in Cartesian space given by the expression

$$D_R^{-1}(\mathbf{q},\omega)=\begin{pmatrix}m\omega^2+i\eta\omega & -i\alpha\omega\\ i\alpha\omega & m\omega^2+i\eta\omega\end{pmatrix}-\Phi_{\mathbf{q}}. \quad (14)$$

We have in Eq. (11) introduced matrix notation in order to suppress the integrations over time and summations over

vortex positions and Cartesian indices. Thus, for example, $\tilde{\mathbf{u}}D_R^{-1}\mathbf{u}$ denotes the expression

$$\sum_{\substack{\mathbf{R}\mathbf{R}'\\ \alpha,\alpha'=x,y}} \int_{-\infty}^{\infty} dt \int_{-\infty}^{\infty} dt' \tilde{u}_\alpha(\mathbf{R},t) \times D_R^{-1\alpha\alpha'}(\mathbf{R},t;\mathbf{R}',t') u_{\alpha'}(\mathbf{R}',t'). \tag{15}$$

The Jacobian $\mathcal{J}=|\delta\boldsymbol{\xi}_{\mathbf{R}t}/\delta\tilde{\mathbf{u}}_{\mathbf{R}'t'}|$, guaranteeing the normalization of the generating functional

$$Z[\mathbf{F},\mathbf{J}=\mathbf{0}]=1, \tag{16}$$

is given by

$$\mathcal{J}\propto\exp\left[-\sum_{\mathbf{R}\alpha\alpha'}\int_{-\infty}^{\infty} dt D^{R\alpha\alpha'}_{\mathbf{R}t;\mathbf{R}t}\frac{\partial^2 V(\mathbf{R}+\mathbf{u}_{\mathbf{R}t})}{\partial x_{\alpha'}\partial x_\alpha}\right], \tag{17}$$

where the proportionality constant is the determinant of the inverse free retarded Green's function, $|(D_R^{-1})^{\alpha\alpha'}_{\mathbf{R}t,\mathbf{R}'t'}|$. In the case of a nonzero mass, $m\neq 0$, the Jacobian is an irrelevant constant,[14] and in the case of zero mass, dropping the Jacobian from the integrand is equivalent to defining the retarded free Green's function to vanish at equal times, $D^R_{tt}=0$, which in turn leads to the full retarded Green's function satisfying the same initial condition. In terms of diagrams, the contribution from the Jacobian exactly cancels the tadpole diagrams.

The average with respect to both the thermal noise and the disorder is immediately performed, and we obtain the averaged functional, dropping the irrelevant Jacobian,

$$Z[f]=\langle\langle\mathcal{Z}\rangle\rangle=\int\mathcal{D}\phi e^{iS[\phi]+if\phi}. \tag{18}$$

We have employed a compact notation for the fields,

$$\phi_{\mathbf{R}t}=(\tilde{\mathbf{u}}_{\mathbf{R}t},\mathbf{u}_{\mathbf{R}t})=(\boldsymbol{\phi}_1(\mathbf{R},t),\boldsymbol{\phi}_2(\mathbf{R},t)), \tag{19}$$

and for the external force and an introduced source $\mathbf{J}(\mathbf{R},t)$,

$$f(\mathbf{R},t)=(\mathbf{F}(\mathbf{R},t),\mathbf{J}(\mathbf{R},t)). \tag{20}$$

The action obtained upon averaging, which we also denote by S, consists of two terms

$$S[\phi]=S_0[\phi]+S_V[\phi]. \tag{21}$$

The first term is quadratic in the field

$$S_0[\phi]=\frac{1}{2}\phi D^{-1}\phi, \tag{22}$$

where the matrix notation now in addition includes the dynamic, or Keldysh, indices; i.e., $\phi D^{-1}\phi$ denotes the expression

$$i\sum_{\substack{\mathbf{R}\mathbf{R}'\\ \alpha\alpha' ij}}\int_{-\infty}^{\infty} dt\int_{-\infty}^{\infty} dt'\,\phi_i^\alpha(\mathbf{R},t) \times D_{ij}^{-1\alpha\alpha'}(\mathbf{R},t;\mathbf{R}',t')\phi_j^{\alpha'}(\mathbf{R}',t'). \tag{23}$$

The inverse free matrix Green's function in Keldysh space,

$$D^{-1}=\begin{pmatrix} D_{11}^{-1} & D_{12}^{-1}\\ D_{21}^{-1} & D_{22}^{-1}\end{pmatrix} =\begin{pmatrix} 2i\eta T\delta(t-t')\delta_{\alpha\alpha'}\delta_{\mathbf{R}\mathbf{R}'} & D_R^{-1}(\mathbf{R},t;\mathbf{R}',t')\\ D_A^{-1}(\mathbf{R},t;\mathbf{R}',t') & 0\end{pmatrix}, \tag{24}$$

is a symmetric matrix in all indices and variables, since the inverse free advanced Green's function is obtained by interchanging Cartesian indices as well as position and time variables:

$$D_A^{-1\alpha'\alpha}(\mathbf{R}',t';\mathbf{R},t)=D_R^{-1\alpha\alpha'}(\mathbf{R},t;\mathbf{R}',t'). \tag{25}$$

The interaction term originating from the disorder is

$$S_V[\phi]=-\frac{i}{2}\sum_{\substack{\mathbf{R}\mathbf{R}'\\ \alpha\alpha'}}\int_{-\infty}^{\infty} dt\int_{-\infty}^{\infty} dt'\,\tilde{u}^\alpha_{\mathbf{R}t}\frac{\partial^2\nu(\mathbf{u}_{\mathbf{R}t}-\mathbf{u}_{\mathbf{R}'t'})}{\partial u^\alpha_{\mathbf{R}t}\partial u^{\alpha'}_{\mathbf{R}t}}\tilde{u}_{\mathbf{R}'t'}^{\alpha'}. \tag{26}$$

The source term introduced in Eq. (10),

$$\mathbf{J}\mathbf{u}=\sum_{\mathbf{R}}\int_{-\infty}^{\infty} dt\mathbf{J}(\mathbf{R},t)\cdot\mathbf{u}(\mathbf{R},t), \tag{27}$$

where the source $\mathbf{J}(\mathbf{R},t)$ coupled to the vortex positions $\mathbf{u}(\mathbf{R},t)$ is added to the action in order to generate the vortex correlation functions. For example, we have for the average position

$$\langle\langle\mathbf{u}_{\mathbf{R}t}\rangle\rangle=-i\left.\frac{\delta Z}{\delta\mathbf{J}_{\mathbf{R}t}}\right|_{\mathbf{J}=\mathbf{0}} \tag{28}$$

and the two-point unconnected Green's function

$$\langle\langle\mathbf{u}_{\mathbf{R}t}\mathbf{u}_{\mathbf{R}'t'}\rangle\rangle=-\frac{\delta^2 Z}{\delta\mathbf{J}_{\mathbf{R}t}\delta\mathbf{J}_{\mathbf{R}'t'}}|_{\mathbf{J}=\mathbf{0}}. \tag{29}$$

Here and in the following we use dyadic notation; i.e., $\mathbf{u}_{\mathbf{R}t}\mathbf{u}_{\mathbf{R}'t'}$ is the Cartesian matrix with the components $u_\alpha(\mathbf{R},t)u_{\alpha'}(\mathbf{R}',t')$.

We note that the presented field-theoretic formulation of the Langevin dynamics is the classical limit of the Schwinger-Keldysh formulation of quantum statistical mechanics of a particle coupled linearly to an Ohmic environment.[15]

A. Effective action

In order to obtain self-consistent equations involving the two-point Green's function in a two-particle-irreducible fashion, we add a two-particle source term K to the action in the generating functional

$$Z[f,K]=\int\mathcal{D}\phi\exp\left(iS[\phi]+if\phi+\frac{i}{2}\phi K\phi\right). \tag{30}$$

The generator of connected Green's functions,

$$W[f,K]=-i\ln Z[f,K], \tag{31}$$

has accordingly derivatives

$$\frac{\delta W}{\delta f_i^\alpha(\mathbf{R},t)} = \overline{\phi}_i^\alpha(\mathbf{R},t) \tag{32}$$

and

$$\frac{\delta W}{\delta K_{ii'}^{\alpha\alpha'}(\mathbf{R},t;\mathbf{R}',t')} = \frac{1}{2}\overline{\phi}_i^\alpha(\mathbf{R},t)\,\overline{\phi}_{i'}^{\alpha'}(\mathbf{R}',t') + \frac{i}{2}G_{ii'}^{\alpha\alpha'}(\mathbf{R},t;\mathbf{R}',t'), \tag{33}$$

where $\overline{\phi}$ is the average field, with respect to the action $S[\phi]+f\phi+\phi K\phi/2$,

$$\overline{\phi}_i^\alpha(\mathbf{R},t) = \int \mathcal{D}\phi\,\phi_i^\alpha(\mathbf{R},t)\exp\left(iS[\phi]+if\phi+\frac{i}{2}\phi K\phi\right), \tag{34}$$

and G is the full connected two-point matrix Green's function:

$$G_{ij} = -\frac{\delta^2 W}{\delta f_i \delta f_j} = -i\begin{pmatrix} \langle\langle \delta\tilde{u}_{\mathbf{R}t}^\alpha \delta\tilde{u}_{\mathbf{R}'t'}^{\alpha'}\rangle\rangle & \langle\langle \delta\tilde{u}_{\mathbf{R}t}^\alpha \delta u_{\mathbf{R}'t'}^{\alpha'}\rangle\rangle \\ \langle\langle \delta u_{\mathbf{R}t}^\alpha \delta\tilde{u}_{\mathbf{R}'t'}^{\alpha'}\rangle\rangle & \langle\langle \delta u_{\mathbf{R}t}^\alpha \delta u_{\mathbf{R}'t'}^{\alpha'}\rangle\rangle \end{pmatrix}, \tag{35}$$

where

$$\delta\mathbf{u}_{\mathbf{R}t} = \mathbf{u}_{\mathbf{R}t} - \langle\langle \mathbf{u}_{\mathbf{R}t}\rangle\rangle \tag{36}$$

and

$$\delta\tilde{\mathbf{u}}_{\mathbf{R}t} = \tilde{\mathbf{u}}_{\mathbf{R}t} - \langle\langle \tilde{\mathbf{u}}_{\mathbf{R}t}\rangle\rangle. \tag{37}$$

In the physical problem of interest, the sources K and $\mathbf{J}$ vanish, $K=0$ and $\mathbf{J}=\mathbf{0}$, and the full matrix Green's function has, due to the normalization of the generating functional

$$Z[\mathbf{F},\mathbf{J}=\mathbf{0},\quad K=\mathbf{0}]=1, \tag{38}$$

the structure in Keldysh space

$$G_{ij} = -i\begin{pmatrix} 0 & \langle\langle \tilde{u}_{\mathbf{R}t}^\alpha u_{\mathbf{R}'t'}^{\alpha'}\rangle\rangle \\ \langle\langle u_{\mathbf{R}t}^\alpha \tilde{u}_{\mathbf{R}'t'}^{\alpha'}\rangle\rangle & \langle\langle \delta u_{\mathbf{R}t}^\alpha \delta u_{\mathbf{R}'t'}^{\alpha'}\rangle\rangle \end{pmatrix} = \begin{pmatrix} 0 & G_{\alpha\alpha'}^A(\mathbf{R},t;\mathbf{R}',t') \\ G_{\alpha\alpha'}^R(\mathbf{R},t;\mathbf{R}',t') & G_{\alpha\alpha'}^K(\mathbf{R},t;\mathbf{R}',t') \end{pmatrix}, \tag{39}$$

where we observe that the connected and unconnected retarded (or advanced) Green's functions are equal. Similarly, in the absence of sources the expectation value of the auxiliary field vanishes, and the average field is therefore given by

$$\overline{\phi}_{\mathbf{R}t} = (\langle\langle \tilde{\mathbf{u}}_{\mathbf{R}t}\rangle\rangle, \langle\langle \mathbf{u}_{\mathbf{R}t}\rangle\rangle) = (\mathbf{0},\mathbf{v}t), \tag{40}$$

where $\mathbf{v}$ is the average velocity of the vortex lattice.

The retarded Green's function $G_{\alpha\alpha'}^R$ yields a linear response to the force $F_{\alpha'}$; i.e., to linear order in the external force we have

$$\langle\langle u_\alpha(\mathbf{R},t)\rangle\rangle = \sum_{\mathbf{R}'}\int_{-\infty}^{\infty} dt' G_{\alpha\alpha'}^R(\mathbf{R},t;\mathbf{R}',t')F_{\alpha'}(\mathbf{R}',t'), \tag{41}$$

and $G_{\alpha\alpha'}^K$ is the correlation function, both matrices in Cartesian indices as indicated. The matrix Green's function in Keldysh space, Eq. (39), has only two independent components, since the advanced Green's function is given by

$$G_{\alpha\alpha'}^A(\mathbf{R},t;\mathbf{R}',t') = G_{\alpha'\alpha}^R(\mathbf{R}',t';\mathbf{R},t). \tag{42}$$

Pursuing an equation for the pinning force, we introduce the effective action Γ, the generator of two-particle-irreducible vertex functions, i.e., the Legendre transform of the generator of connected Green's functions, W,

$$\Gamma[\overline{\phi},G] = W[f,K] - f\overline{\phi} - \frac{1}{2}\overline{\phi}K\overline{\phi} - \frac{i}{2}\,\mathrm{Tr}\,GK, \tag{43}$$

where Tr denotes the trace over all variables and indices; i.e., $\mathrm{Tr}\,GK$ denotes the expression

$$\sum_{\substack{\mathbf{R},\mathbf{R}'\\ \alpha,\alpha'=x,y\\ i,i'=1,2}} \int_{-\infty}^{\infty} dt \int_{-\infty}^{\infty} dt' G_{ii'}^{\alpha\alpha'}(\mathbf{R},t;\mathbf{R}',t')K_{i'i}^{\alpha'\alpha}(\mathbf{R}',t';\mathbf{R},t). \tag{44}$$

The effective action satisfies the equations

$$\frac{\delta\Gamma}{\delta\overline{\phi}} = -f - K\overline{\phi} \tag{45}$$

and

$$\frac{\delta\Gamma}{\delta G} = -\frac{i}{2}K. \tag{46}$$

The effective action can be written on the form[10]

$$\Gamma[\overline{\phi},G] = S[\overline{\phi}] + \frac{i}{2}\,\mathrm{Tr}\,D_S^{-1}G - \frac{i}{2}\mathrm{Tr}\ln D^{-1}G - \frac{i}{2}\mathrm{Tr}\,1 - i\ln\langle e^{iS_{\mathrm{int}}[\overline{\phi},\psi]}\rangle_G^{\mathrm{2PI}}, \tag{47}$$

where the quantity D_S^{-1} is the second derivative of the action at the average field,

$$D_S^{-1}[\overline{\phi}](t,t') = \frac{\delta^2 S[\overline{\phi}]}{\delta\overline{\phi}_t\delta\overline{\phi}_{t'}}, \tag{48}$$

and $S_{\mathrm{int}}[\overline{\phi},\psi]$ is the part of the action $S[\overline{\phi}+\psi]$ which is higher than second order in ψ in an expansion around the average field. The superscript ''2PI'' on the last term indicates that only the two-particle irreducible vacuum diagrams should be included in the interaction part of the effective action, the last term in Eq. (47), and the subscript that propagator lines represent G; i.e., the brackets with subscript G denote the average

$$\langle e^{iS_{\mathrm{int}}[\overline{\phi},\psi]}\rangle_G = (\det iG)^{-1/2}\int \mathcal{D}\psi e^{i\psi G^{-1}\psi/2}e^{iS_{\mathrm{int}}[\overline{\phi},\psi]}. \tag{49}$$

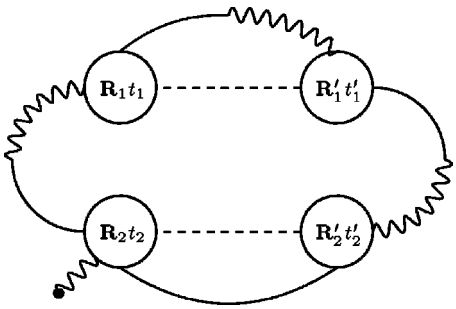

FIG. 1. Typical vacuum diagram not included in the Hartree approximation for the effective action. The solid line represents the correlation function or Keldysh component G^K of the matrix Green's function. The retarded Green's function G^R is depicted as a wiggly line ending up in a straight line, and vice versa for the advanced Green's function G^A. The curly line ending up on the dot represents the first Keldysh component of the average field. A dashed line attached to circles represents the impurity correlator and the additional dependence on the second component of the average field as explicitly specified in Eq. (51).

B. Hartree approximation

In order to obtain a closed expression for the self-energy in terms of the two-point Green's function, we expand the exponential and keep only the lowest-order term

$$-i\ln\langle e^{iS_{\rm int}[\overline{\phi},\psi]}\rangle_G^{\rm 2PI}\simeq -i\ln\langle 1+iS_{\rm int}[\overline{\phi},\psi]\rangle_G^{\rm 2PI}$$
$$\simeq\langle S_{\rm int}[\overline{\phi},\psi]\rangle_G; \tag{50}$$

i.e., we consider the Hartree approximation, which in diagrammatic terms corresponds to neglecting diagrams where different impurity correlators are connected by Green's functions. A typical vacuum diagram not included in the Hartree approximation for the effective action is shown in Fig. 1, and represents the expression

$$\left(\frac{i}{2}\right)^2\left(\frac{1}{4!}\right)^2\int\frac{d\mathbf{k}_1}{(2\pi)^2}\frac{d\mathbf{k}_2}{(2\pi)^2}\mathbf{k}_2\cdot\overline{\boldsymbol{\phi}}_1(\mathbf{R}_2,t_2)$$
$$\times[\mathbf{k}_2G^R(\mathbf{R}_2,t_2;\mathbf{R}_1,t_1)\mathbf{k}_1][\mathbf{k}_1G^R(\mathbf{R}_1,t_1;\mathbf{R}_1',t_1')\mathbf{k}_1]$$
$$\times[\mathbf{k}_1G^R(\mathbf{R}_1',t_1';\mathbf{R}_2',t_2')\mathbf{k}_2][\mathbf{k}_2G^K(\mathbf{R}_2,t_2;\mathbf{R}_2',t_2')\mathbf{k}_2]$$
$$\times\nu(\mathbf{k}_1)e^{i\mathbf{k}_1\cdot[\mathbf{R}_1-\mathbf{R}_1'+\mathbf{v}(t_1-t_1')]}\nu(\mathbf{k}_2)$$
$$\times e^{i\mathbf{k}_2\cdot[\mathbf{R}_2-\mathbf{R}_2'+\mathbf{v}(t_2-t_2')]}, \tag{51}$$

where integrations over time and summations over vortex positions are implied, and we have introduced the notation

$$\mathbf{k}G^R(\mathbf{R},t;\mathbf{R}',t')\mathbf{k}'=\sum_{\alpha\alpha'}k_\alpha G^R_{\alpha\alpha'}(\mathbf{R},t;\mathbf{R}',t')k'_{\alpha'} \tag{52}$$

for Cartesian scalars.

In the Hartree approximation, Eq. (50), we can drop the superscript ''2PI'' since the action $S_{\rm int}[\overline{\phi},\psi]$ only generates two-particle-irreducible vacuum diagrams, due to the appearance of only one impurity correlator. The Hartree approximation can also be expressed as a Gaussian fluctuation corrected saddle-point approximation.[16]

The effective action can in the Hartree approximation be rewritten in the form

$$\Gamma[\overline{\phi},G]=S_0[\overline{\phi}]-\frac{i}{2}\,\mathrm{Tr}\ln D^{-1}G+\frac{i}{2}\,\mathrm{Tr}\,D^{-1}G-\frac{i}{2}\,\mathrm{Tr}\,1$$
$$+\langle S_V[\overline{\phi}+\psi]\rangle_G, \tag{53}$$

since

$$\langle S_{\rm int}[\overline{\phi},\psi]\rangle_G=\langle S_V[\overline{\phi}+\psi]\rangle_G-S_V[\overline{\phi}]$$
$$-\frac{i}{2}\,\mathrm{Tr}\int_{-\infty}^{\infty}dt\int_{-\infty}^{\infty}dt'\,\frac{\delta^2S_V[\overline{\phi}]}{\delta\overline{\phi}_t\delta\overline{\phi}_{t'}}\,G_{t't}, \tag{54}$$

where the trace in the time variable has been written explicitly for clarity.

In the physical situation of interest the two-particle source K vanishes, and since Γ is two-particle irreducible, Eq. (46) therefore becomes the Dyson equation

$$G^{-1}=D^{-1}-\Sigma, \tag{55}$$

where the self-energy in the Hartree approximation is the matrix in Keldysh space:

$$\Sigma_{ij}=\begin{pmatrix}\Sigma^K & \Sigma^R\\ \Sigma^A & 0\end{pmatrix}=2i\,\frac{\delta\langle S_V[\overline{\phi}+\psi]\rangle_G}{\delta G_{ij}}\bigg|_{K=0,\ \mathbf{J}=\mathbf{0}}. \tag{56}$$

The Dyson equation, Eq. (55), the self-energy expression, Eq. (56), and the equation relating the effective action to the external force, Eq. (45), constitute a set of self-consistent equations for the Green's functions, the self-energies, and the average field.

The matrix self-energy in Keldysh space has only two independent components since

$$\Sigma^A_{\alpha\alpha'}(\mathbf{R},t;\mathbf{R}',t')=\Sigma^R_{\alpha'\alpha}(\mathbf{R}',t';\mathbf{R},t), \tag{57}$$

a simple consequence of Eq. (42) and the Dyson equation. From Eq. (56) we obtain for a vortex lattice having a unit cell of area a^2 and consisting of N vortices, the self-energy components (each a matrix in Cartesian space)

$$\Sigma^K(\mathbf{R},t;\mathbf{R}',t')=-\frac{i}{Na^2}\sum_{\mathbf{k}}\nu(\mathbf{k})\mathbf{k}\mathbf{k}e^{-\tilde{\varphi}(\mathbf{R},t;\mathbf{R}',t';\mathbf{k};\mathbf{v})} \tag{58}$$

and

$$\Sigma^R(\mathbf{R},t;\mathbf{R}',t')$$
$$=\sigma^R(\mathbf{R},t;\mathbf{R}',t')-\delta_{\mathbf{R}\mathbf{R}'}\delta(t-t')$$
$$\times\sum_{\tilde{\mathbf{R}}}\int_{-\infty}^{\infty}d\tilde{t}\,\sigma^R(\mathbf{R},t;\tilde{\mathbf{R}},\tilde{t}), \tag{59}$$

where

$$\sigma^R(\mathbf{R},t;\mathbf{R}',t') = \frac{1}{Na^2}\sum_{\mathbf{k}} \nu(\mathbf{k})\mathbf{kk}[\mathbf{k}G^R(\mathbf{R},t;\mathbf{R}',t')\mathbf{k}]e^{-\tilde{\varphi}(\mathbf{R},t;\mathbf{R}',t';\mathbf{k};\mathbf{v})}. \tag{60}$$

We use dyadic notation; i.e., $\mathbf{kk}$ denotes the matrix with the Cartesian components $k_\alpha k_{\alpha'}$. The influence of thermal and disorder-induced fluctuations is described by the fluctuation or damping exponent

$$\varphi_{\mathbf{k}}(\mathbf{R},t;\mathbf{R}',t') = i\mathbf{k}[G^K(\mathbf{R},t;\mathbf{R},t) - G^K(\mathbf{R},t;\mathbf{R}',t')]\mathbf{k} \tag{61}$$

contained in

$$\tilde{\varphi}(\mathbf{R},t;\mathbf{R}',t';\mathbf{k};\mathbf{v}) = -i\mathbf{k}\cdot[\mathbf{R}-\mathbf{R}'+\mathbf{v}(t-t')] + \varphi_{\mathbf{k}}(\mathbf{R},t;\mathbf{R}',t'). \tag{62}$$

The pinning force on a vortex, Eq. (7), is determined by the averaged equation of motion, Eq. (6), and the first Keldysh component of Eq. (45), which in the Hartree approximation yields

$$-\sum_{\mathbf{R}'}\sum_{\alpha'}\int_{-\infty}^{\infty} dt' D_R^{-1\alpha\alpha'}(\mathbf{R},t;\mathbf{R}',t')v_{\alpha'}t' = F_{\mathbf{R}}^{\alpha} + \left.\frac{\delta\langle S_V[\bar{\phi}+\psi]\rangle_G}{\delta\bar{\phi}_1^{\alpha}(\mathbf{R},t)}\right|_{\bar{\phi}_{\mathbf{R}t}=(\mathbf{0},\mathbf{v}t)}, \tag{63}$$

resulting in the expression for the pinning force:

$$\mathbf{F}_p = i\sum_{\mathbf{R}'}\int_{-\infty}^{\infty} dt' \int \frac{d\mathbf{k}}{(2\pi)^2}\mathbf{k}\nu(\mathbf{k}) \times(\mathbf{k}G^R_{\mathbf{R}t\mathbf{R}'t'}\mathbf{k})e^{-\tilde{\varphi}(\mathbf{R},t;\mathbf{R}',t';\mathbf{k};\mathbf{v})}. \tag{64}$$

The self-consistent theory is still intractable to analytical treatment, except in the limiting cases considered in the following, but it is manageable numerically. In the following we shall study numerically the vortex dynamics in the Hartree approximation. The results obtained from the self-consistent theory will then be compared to analytical results obtained in perturbation theory and to simulations of the vortex dynamics.

IV. SINGLE VORTEX

In order to study the essential features of the model and the self-consistent method, we first consider the case of a single vortex, since this example will allow the important test of comparing the results of the self-consistent theory with simulations. The dynamics of a single vortex is described by the Langevin equation

$$m\ddot{\mathbf{x}}_t + \eta\dot{\mathbf{x}}_t = -\nabla V(\mathbf{x}_t) + \mathbf{F}_t + \boldsymbol{\xi}_t, \tag{65}$$

where $\mathbf{x}_t$ is the vortex position at time t. We defer the discussion of the Hall force to Sec. IV E.

When presenting analytical and numerical results obtained from the self-consistent theory, we shall always choose the vortex mass (per unit length) to be small, in fact so small, $m \ll \eta^2 r_p^3/\sqrt{\nu_0}$, that the case of zero mass only deviates slightly from the presented results, i.e., at most a few percent.

A. Perturbation theory

At high velocities, the pinning force can be obtained from lowest-order perturbation theory in the disorder, since the pinning force then is small compared to the friction force, and only makes, according to Eq. (6), a small contribution to the total force on the vortex. We first consider the case of zero temperature, where we obtain the following set of equations by collecting terms of equal powers in the pinning potential:

$$-\int_{-\infty}^{\infty} dt' D_R^{-1}(t,t')\mathbf{x}_{t'}^{(0)} = \mathbf{F}_t, \tag{66a}$$

$$-\int_{-\infty}^{\infty} dt' D_R^{-1}(t,t')\mathbf{x}_{t'}^{(1)} = -\nabla V(\mathbf{x}_t^{(0)}), \tag{66b}$$

$$-\int_{-\infty}^{\infty} dt' D_R^{-1}(t,t')\mathbf{x}_{t'}^{(2)} = -\nabla(\mathbf{x}_t^{(1)}\cdot\nabla V(\mathbf{x}_t^{(0)})). \tag{66c}$$

Assuming that the external force is independent of time, the average vortex velocity will be constant in time, and in the absence of disorder the average vortex position is

$$\langle\langle\mathbf{x}_t^{(0)}\rangle\rangle = \mathbf{v}t = \frac{\mathbf{F}t}{\eta}; \tag{67}$$

i.e., the friction force balances the external force, $\eta\mathbf{v}=\mathbf{F}$. The first-order contribution to the vortex position vanishes upon averaging with respect to the pinning potential, and the second-order contribution to the average vortex velocity becomes, according to Eqs. (66),

$$\langle\langle\dot{\mathbf{x}}_t^{(2)}\rangle\rangle = -\frac{i}{\eta}\int_{-\infty}^{\infty} dt' D_{tt'}^R \int \frac{d\mathbf{k}}{(2\pi)^2}\mathbf{k}k^2\nu_0 e^{-k^2r_p^2 + i\mathbf{k}\cdot\mathbf{v}(t-t')} = \frac{\nu_0}{4\pi r_p^5\eta}\int_0^{\infty} dt D_{t0}^R\left[\frac{vt}{r_p} - \left(\frac{vt}{2r_p}\right)^2\right]e^{-(vt/2r_p)^2}. \tag{68}$$

The second-order contribution is immediately calculated, and for example for the case of a vanishing mass $m \ll \eta^2 r_p^3/\sqrt{\nu_0}$, we obtain

$$\langle\langle\dot{\mathbf{x}}_t^{(2)}\rangle\rangle = -\frac{\nu_0}{4\pi r_p^4\eta^2 v^2}\mathbf{v}. \tag{69}$$

The pinning force is then, according to Eq. (6), to lowest order in the disorder strength ν_0, given by

$$\mathbf{F}_p = -\frac{\nu_0}{4\pi r_p^4\eta v^2}\mathbf{v}; \tag{70}$$

i.e., the magnitude of the pinning force is inversely proportional to the magnitude of the velocity. The perturbation re-

sult is therefore valid for large velocities $v \gg \sqrt{\nu_0}/\eta r_p^2$, i.e., when the friction force is much larger than the average force $\sqrt{\nu_0}/r_p^2$ due to the disorder.

B. Self-consistent theory

The self-energy equations for a single vortex reduce in the Hartree approximation to

$$\Sigma^R(t,t') = \int \frac{d\mathbf{k}}{(2\pi)^2}\left[\sigma_{\mathbf{k}}^R(t,t') - \delta(t-t')\int_{-\infty}^{\infty} d\bar{t}\,\sigma_{\mathbf{k}}^R(t,\bar{t})\right], \tag{71a}$$

$$\sigma_{\mathbf{k}}^R(t,t') = \nu(\mathbf{k})\mathbf{k}\mathbf{k}[\mathbf{k}G^R(t,t')\mathbf{k}]e^{i\mathbf{k}\cdot\mathbf{v}(t-t')-\varphi_{\mathbf{k}}(t,t')}, \tag{71b}$$

$$\Sigma^K(t,t') = -i\int \frac{d\mathbf{k}}{(2\pi)^2}\nu(\mathbf{k})\mathbf{k}\mathbf{k}e^{i\mathbf{k}\cdot\mathbf{v}(t-t')-\varphi_{\mathbf{k}}(t,t')}, \tag{71c}$$

with the fluctuation exponent

$$\varphi_{\mathbf{k}}(t,t') = i\mathbf{k}[G^K(t,t) - G^K(t,t')]\mathbf{k}. \tag{72}$$

Writing out the components of the Keldysh matrix Dyson equation, Eq. (55), we obtain the Cartesian matrix Green's functions

$$G^K(\omega) = G^R(\omega)[\Sigma^K(\omega) - 2i\eta T 1]G^A(\omega) \tag{73}$$

and

$$G^R(\omega) = \frac{\hat{\mathbf{v}}\hat{\mathbf{v}}}{m\omega^2 + i\eta\omega - \Sigma_{\parallel}^R(\omega)} + \frac{1-\hat{\mathbf{v}}\hat{\mathbf{v}}}{m\omega^2 + i\eta\omega - \Sigma_{\perp}^R(\omega)}, \tag{74}$$

where the subscripts $\parallel$ and $\perp$ denote longitudinal and transverse components of the retarded self-energy with respect to the direction of the velocity:

$$\Sigma_{\parallel}^R(\omega) = \sum_{\alpha,\alpha'} \hat{v}_\alpha \Sigma_{\alpha\alpha'}^R(\omega)\hat{v}_{\alpha'} \tag{75}$$

and

$$\Sigma_{\perp}^R(\omega) = \sum_{\alpha,\alpha'} \Sigma_{\alpha\alpha'}^R(\omega)(\delta_{\alpha\alpha'} - \hat{v}_\alpha\hat{v}_{\alpha'}). \tag{76}$$

The advanced Green's function is obtained from the retarded by complex conjugation and interchange of Cartesian indices:

$$G_{\alpha\alpha'}^A(\omega) = [G_{\alpha'\alpha}^R(\omega)]^*. \tag{77}$$

The expression for the pinning force, Eq. (64), reduces for a single vortex to

$$\mathbf{F}_p = i\int_{-\infty}^{\infty} dt' \int \frac{d\mathbf{k}}{(2\pi)^2}\mathbf{k}\nu(\mathbf{k})(\mathbf{k}G_{tt'}^R\mathbf{k})e^{i\mathbf{k}\cdot\mathbf{v}(t-t')-\varphi_{\mathbf{k}}(t,t')}. \tag{78}$$

The previous discussion of the high-velocity regime, where lowest-order perturbation theory in the disorder is valid, can be generalized to nonzero temperature. At high velocities $v \gg \sqrt{\nu_0}/\eta r_p^2$, the self-energies are according to Eqs. (71) inversely proportional to the velocity, and they can accordingly be neglected in the calculation of the pinning force. We can therefore in this limit insert the free retarded Green's functions in the self-consistent expression for the pinning force, Eq. (78), thereby obtaining an expression valid to lowest order in the disorder strength ν_0,

$$\mathbf{F}_p = -\frac{i}{\eta}\int \frac{d\mathbf{k}}{(2\pi)^2}\mathbf{k}k^2\nu_0 e^{-r_p^2k^2}\int_0^{\infty} dt e^{i\mathbf{k}\cdot\mathbf{v}t - k^2Tt/\eta}, \tag{79}$$

where again we only display the result for vanishing mass, $m \ll \eta^2 r_p^3/\sqrt{\nu_0}$. The integration over time can then be performed, and we obtain that the pinning force for large velocities $v \gg T/(r_p\eta)$ is given by the perturbation theory expression, Eq. (70).

It is also possible to obtain an analytical expression for the pinning force at moderate velocities, provided the temperature is high enough. At high temperatures $T \gg \sqrt{\nu_0}/r_p$, the Keldysh component of the self-energy is inversely proportional to the temperature, $\Sigma^K(\omega = v/r_p) \sim \nu_0\eta/(r_p^2 T)$, and its contribution to the fluctuation exponent is much smaller than the contribution from the thermal fluctuations. Similarly, at temperatures $T \gg \sqrt{\nu_0}/(\eta r_p^3 v)$, the retarded self-energy is of order $\Sigma^R(\omega = v/r_p) \sim \nu_0/(r_p^4 T)$. At moderate velocities $v \ll \sqrt{\nu_0}/(\eta r_p^2)$, the free retarded Green's function can therefore be inserted in the expression for the pinning force, and we can expand the exponential $\exp\{i\mathbf{k}\cdot\mathbf{v}t\}$, and keep only the lowest-order term in the velocity, since the inequality $v \ll T/(\eta r_p)$ is satisfied, and obtain that the pinning force is proportional to the velocity and inversely proportional to the square of the temperature:

$$\mathbf{F}_p = -\frac{\nu_0\eta}{8\pi r_p^2 T^2}\mathbf{v}. \tag{80}$$

Thus, when the thermal energy exceeds the average disorder barrier height $\sqrt{\nu_0}/r_p$, the pinning force is very small compared to the friction force, and pinning just leads to a slight renormalization of the bare friction coefficient. In this high-temperature limit, which can be realized in high-temperature superconductors, we observe that the self-consistent theory, at not too high velocities, yields a pinning force that has a linear velocity dependence, in contrast to the case of low temperatures where we obtain from the self-consistent theory, as apparent from, for example, Fig. 2, that the velocity dependence of the pinning force is sublinear.

C. Simulations

In order to ascertain the validity of the self-consistent theory beyond the high-velocity regime, where perturbation theory is valid, we perform numerical simulations of the Langevin equation, Eq. (65). The pinning force is obtained from Eq. (6), once the simulation result for the average velocity as a function of the external force is determined. We simulate the two-dimensional motion of a vortex in a region of linear size $L = 20r_p$, and use periodic boundary conditions. The disorder is generated on a grid consisting of 1024×1024 points.

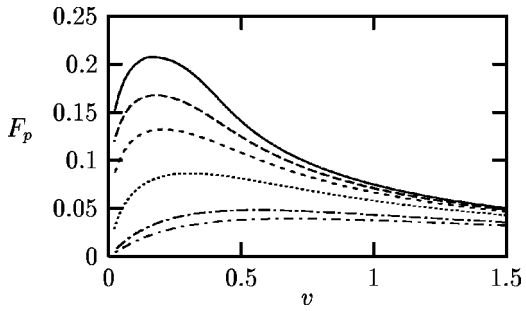

FIG. 2. Pinning force (in units of $\nu_0^{1/2} r_p^{-2}$) on a single vortex as a function of velocity (in units of $\eta^{-1} r_p^{-2} \nu_0^{1/2}$) obtained from the self-consistent theory. The curves correspond to the different temperatures $T=0.005,0.05,0.1,0.2,0.4,0.5$ (in units of $\nu_0^{1/2}/r_p$), where the uppermost curve corresponds to $T=0.005$, and $m=0.1\eta^2 r_p^3 \nu_0^{-1/2}$.

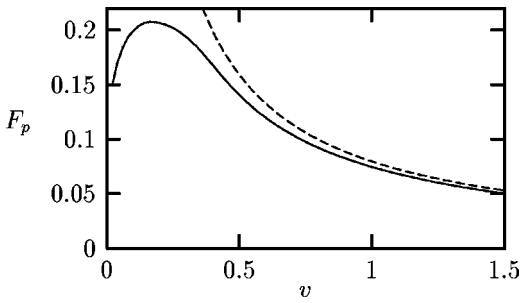

FIG. 3. Pinning force (in units of $\nu_0^{1/2} r_p^{-2}$) on a single vortex as a function of velocity (in units of $\eta^{-1} r_p^{-2} \nu_0^{1/2}$). The solid line represents the result obtained from the self-consistent theory, while the dashed line represents the result of lowest order perturbation theory in the disorder ($T=0.005\nu_0^{1/2} r_p^{-1}$ and $m=0.1\eta^2 r_p^3 \nu_0^{-1/2}$).

The disorder correlator is diagonal in the wave vectors, since averaged quantities are translationally invariant,

$$\langle V(\mathbf{k}) V(\mathbf{k}') \rangle = \nu(\mathbf{k}) L^2 \delta_{\mathbf{k}+\mathbf{k}'=\mathbf{0}}, \tag{81}$$

and the real and imaginary parts of the disorder potential can be generated independently according to

$$\mathrm{Re}\, V(\mathbf{k}) = \frac{\sqrt{\nu_0} L}{\sqrt{2}} e^{-r_p^2 k^2/2} \sigma, \tag{82a}$$

$$\mathrm{Im}\, V(\mathbf{k}) = \frac{\sqrt{\nu_0} L}{\sqrt{2}} e^{-r_p^2 k^2/2} \delta, \tag{82b}$$

where σ and δ are normally distributed stochastic variables with zero mean and unit standard deviation. The gradient of the disorder potential at the grid points is obtained by employing the finite difference scheme. The potential gradient at the vortex position is then obtained by interpolation of the values of the potential at the four nearest grid points.

The simulations show that the vortex follows a fairly narrow channel through the potential landscape. In the absence of the Hall force, the vortex will traverse only a very limited region of the generated potential due to the imposed periodic boundary condition. To make better use of the generated potential, we therefore randomize the vortex position at equidistant moments in time, and run the simulation for a short time without measuring the velocity, in order for the velocity to relax, before again starting to measure the velocity. In this way the number of generated potentials can be kept at a minimum of 20.

D. Numerical results

For any given average velocity of the lattice, the coupled equations of Green's functions and self-energies may be solved numerically by iteration: We start the iteration procedure by first calculating the Green's functions for vanishing self-energies, corresponding to the absence of disorder, and the self-energies are then calculated from Eqs. (71). The procedure is then iterated until convergence is reached. The pinning force on a single vortex can then be evaluated numerically from Eq. (78).

In the numerical calculations we shall always assume that the correlator of the pinning potential is the Gaussian function, Eq. (9), with range r_p and strength ν_0. In order to simplify the numerical calculation, the self-consistent equations for the self-energies and the Green's functions, Eqs. (71), Eq. (73), and Eq. (74), are brought to dimensionless form by introducing the following units for length, time, and mass: r_p, $\eta r_p^3/\nu_0^{1/2}$, and $\eta^2 r_p^4/\nu_0^{1/2}$.

We have solved the set of self-consistent equations numerically by iteration. In Fig. 2, the pinning force as a function of velocity is shown for different values of the temperature. We find that the pinning force has a nonmonotonic dependence as a function of velocity, and that the peak in the pinning force decreases rapidly with increasing temperature, and develops into a plateau once the thermal energy is of the order of the average barrier height. At the highest temperature, the velocity dependence of the pinning force is seen in Fig. 2 to approach the linear regime at low velocities in accordance with the analytical result obtained in the high-temperature limit, Eq. (80). At high velocities, the pinning force is independent of the temperature as apparent from Fig. 2. In fact, the pinning force is inversely proportional to the velocity at high velocities in agreement with the perturbation theory result, Eq. (70), as apparent from Fig. 3, where a comparison is made between the pinning force obtained from lowest-order perturbation theory and the numerically evaluated self-consistent result. The two results agree as expected in the large velocity regime, whereas the perturbation theory result has an unphysical divergence at low velocities due to the neglect of fluctuations and a consequent absence of damping by the fluctuation exponent in Eq. (78).

In order to check the validity of the self-consistent theory beyond lowest-order perturbation theory, we have performed numerical simulations. In Fig. 4, a comparison between the self-consistent theory and a numerical simulation of the pinning force as a function of velocity is presented. The agreement between the self-consistent theory and the simulation is good, except around the maximum value of the pinning force, where the simulation is found to yield a higher pinning force in comparison to the self-consistent theory. In this region the relative velocity fluctuations are large, and in fact the self-consistent theory predicts that the relative velocity fluctuations are diverging at zero velocity even at zero temperature, as we discuss shortly. The self-consistent equations

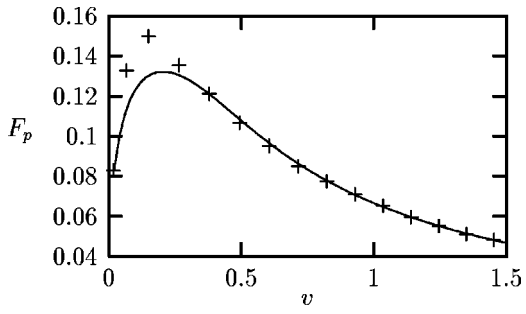

FIG. 4. Comparison of the pinning force (in units of $\nu_0^{1/2} r_p^{-2}$) on a single vortex as a function of velocity (in units of $\eta^{-1} r_p^{-2} \nu_0^{1/2}$) obtained from the self-consistent theory, solid line, and the numerical simulation, plus signs, ($T = 0.1 \nu_0^{1/2} r_p^{-1}$ and $m = 0.1 \eta^2 r_p^3 \nu_0^{-1/2}$).

and their numerical solution, as well as the simulations, can therefore be expected to be less accurate at low velocities.

The convergence of the iterative procedure can be monitored by checking that energy conservation is fulfilled. The energy conservation relation is obtained by multiplying the Langevin equation by the velocity of the vortex and averaging over the thermal noise and the quenched disorder:

$$m\langle\langle \dot{\mathbf{x}}_t \cdot \ddot{\mathbf{x}}_t \rangle\rangle + \eta \langle\langle \dot{\mathbf{x}}_t^2 \rangle\rangle = -\langle\langle \dot{\mathbf{x}}_t \cdot \nabla V(\mathbf{x}_t) \rangle\rangle + \mathbf{F} \cdot \mathbf{v} + \langle\langle \dot{\mathbf{x}}_t \cdot \boldsymbol{\xi}_t \rangle\rangle. \tag{83}$$

The first term is proportional to $\partial_t \langle\langle \dot{\mathbf{x}}_t^2 \rangle\rangle$, and vanishes since averaged quantities are independent of time, as the external force is assumed to be independent of time. The first term on the right side, the term originating from the disorder, vanishes for the same reason, since it can be rewritten as $-\partial_t \langle\langle V(\mathbf{x}_t) \rangle\rangle$. The energy conservation relation therefore becomes, $\mathbf{v} = \langle\langle \dot{\mathbf{x}}_t \rangle\rangle$,

$$\eta \langle\langle (\dot{\mathbf{x}}_t - \mathbf{v})^2 \rangle\rangle - \langle\langle \dot{\mathbf{x}}_t \cdot \boldsymbol{\xi}_t \rangle\rangle = -\mathbf{v} \cdot \mathbf{F}_p \tag{84}$$

or, in terms of the Green's functions,

$$-i\eta \partial_t^2 \operatorname{tr} G^K_{tt'}|_{t'=t} + 2\eta T \partial_t \operatorname{tr} G^R_{tt'}|_{t'=t} = -\mathbf{v} \cdot \mathbf{F}_p, \tag{85}$$

where tr denotes the trace with respect to the Cartesian indices. The energy conservation relation simply states that on the average the work performed by the external and thermal noise forces is dissipated due to friction.

In order to ascertain the convergence of the iteration process, employed when solving the self-consistent equations, we test how accurately the iterated solution satisfies the energy conservation relation. In Fig. 5 the velocity dependence of the left and right sides of the energy conservation relation, Eq. (85), is shown. After at the most 20 iterations, the energy conservation relation is satisfied by the iterated solution to within an accuracy of 1%.

In Sec. VI we shall consider dynamic melting of the vortex lattice, and it is therefore of interest to check the validity of the fluctuations predicted by the self-consistent theory against direct simulations of the Langevin equation. In order to check the accuracy of the velocity fluctuations calculated within the self-consistent theory, we have performed simulations of the velocity fluctuations. In Fig. 6, the velocity fluctuations obtained from the self-consistent theory are compared to simulations. The agreement between the self-consistent theory and the numerical simulations is seen to be

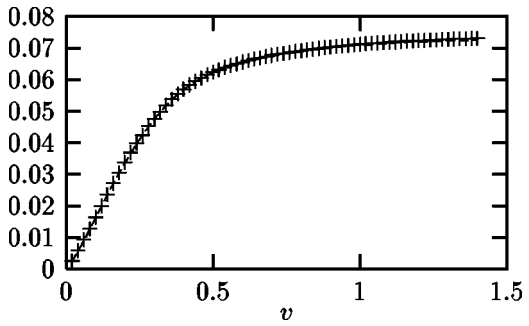

FIG. 5. The values (in units of $\nu_0 \eta^{-1} r_p^{-4}$) of the expressions on the two sides of the energy conservation relation, Eq. (85), are shown as a function of the velocity (in units of $\eta^{-1} r_p^{-2} \nu_0^{1/2}$). The dashed line and the plus symbols correspond to the left and right sides, respectively ($T = 0.05 \nu_0^{1/2} r_p^{-1}$ and $m = 0.1 \eta^2 r_p^3 \nu_0^{-1/2}$). The energy conservation relation is fulfilled to within an accuracy of 1%.

good, indicating that fluctuations calculated from the self-consistent theory are quantitatively correct. The velocity fluctuations approach at low average velocities their thermal value T/m. The relative velocity fluctuations diverge at zero velocity even at zero temperature. This can be inferred from the energy conservation relation, Eq. (84), and the sublinear velocity dependence of the pinning force at low velocities, as, for example, apparent from Fig. 2. At intermediate average velocities, the velocity fluctuations in the direction parallel to the average velocity (chosen along the $\hat{\mathbf{x}}$ axis), the longitudinal velocity fluctuations $\langle\langle (\dot{x}_t - v)^2 \rangle\rangle$, are found to be larger than the fluctuations perpendicular to the average velocity, the transverse velocity fluctuations $\langle\langle \dot{y}_t^2 \rangle\rangle$. The reason behind this is that at not too high velocities, where the force due to the disorder is strong compared to the friction

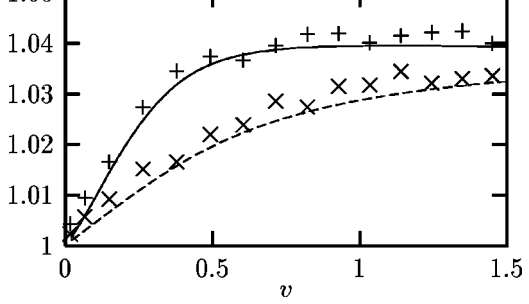

FIG. 6. Longitudinal and transverse velocity fluctuations (in units of $\eta^{-2} r_p^{-4} \nu_0$) as a function of the average velocity (in units of $\eta^{-1} r_p^{-2} \nu_0^{1/2}$). The solid and dashed lines represent the results for the longitudinal (parallel to the external force), $\langle\langle (\dot{x}_t - v)^2 \rangle\rangle$, and transverse, $\langle\langle \dot{y}_t^2 \rangle\rangle$, velocity fluctuations obtained from the self-consistent theory, respectively. The plus signs and crosses represent the simulation results for the longitudinal and transverse velocity fluctuations, respectively ($T = 0.1 \nu_0^{1/2} r_p^{-1}$ and $m = 0.1 \eta^2 r_p^3 \nu_0^{-1/2}$). At low average velocities the fluctuations approach their thermal value, T/m, which for the parameters and units in question equal 1. At intermediate average velocities the longitudinal velocity fluctuations are larger than the transverse, due to the jerky motion of the particle along the preferred direction of the external force, before reaching the same value at high average velocities where the effect of the disorder simply acts as an additional contribution to the temperature.

force, the motion of the particle is jerky since the particle slowly makes it to the disorder potential tops, and subsequently are accelerated by the disorder potential. Since the average motion of the particle is due to the external driving force, the jerky motion and, thereby, the velocity fluctuations are largest in that preferred direction. At high average velocity, the longitudinal and transverse velocity fluctuations saturate and are seen to become equal, due to the strong friction force causing a steadier motion. In this connection we should also mention that we have noticed from our numerical calculations that the second term on the left side of Eq. (84) is independent of the average velocity (and disorder), as is also apparent by comparing Figs. 5 and 6. This thermal fluctuation contribution to the velocity fluctuations is therefore given by its zero-velocity value, and is according to Eq. (84) specified by the equilibrium velocity fluctuations and therefore determined by equipartition. The saturation value of the velocity fluctuations can therefore be determined from the energy conservation relation, Eq. (84). For example, in the case of a small vortex mass, $m \ll \eta^2 r_p^3/\sqrt{\nu_0}$, we can use the high-velocity expression for the pinning force, Eq. (70), and obtain that the saturation value equals $T/m+\nu_0/8\pi r_p^4\eta^2$, a result in good agreement with Fig. 6. At high average velocity, the velocity fluctuations saturate, and the effect of the disorder simply acts as an additional contribution to the temperature.

E. Hall force

In this section the effect of a Hall force is considered, and the previous analysis of the dynamics of a single vortex is extended to include the Hall force:

$$m\ddot{\mathbf{x}}_t+\eta\dot{\mathbf{x}}_t=\alpha\dot{\mathbf{x}}_t\times\hat{\mathbf{z}}-\nabla V(\mathbf{x}_t)+\mathbf{F}_t+\xi_t. \tag{86}$$

We shall use the self-consistent theory to calculate the pinning force, the velocity fluctuations, and the Hall angle

$$\theta=\arctan\frac{F_H}{\hat{\mathbf{v}}\cdot\mathbf{F}}=\arctan\frac{\alpha}{\eta_{\rm eff}}, \tag{87}$$

which can be expressed in terms of the effective friction coefficient.

1. Analytical results

The inverse of the free retarded Green's function acquires according to Eq. (86) off-diagonal elements

$$D_R^{-1}(\omega)=\begin{pmatrix} m\omega^2+i\eta\omega & -i\alpha\omega \\ i\alpha\omega & m\omega^2+i\eta\omega \end{pmatrix}, \tag{88}$$

and the free retarded Green's function is given by

$$D_\omega^R=\frac{1}{(\omega+i0)[(m\omega+i\eta)^2-\alpha^2]}\begin{pmatrix} m\omega+i\eta & i\alpha \\ -i\alpha & m\omega+i\eta \end{pmatrix}. \tag{89}$$

In the high-velocity regime $v \gg \sqrt{\nu_0}/(\eta r_p^2)$, where lowest-order perturbation theory in the disorder is valid, we can neglect the self-energies in the self-consistent expression for the pinning force, Eq. (78); i.e., we can insert the free retarded Green's function and neglect the fluctuation exponent. Since the free retarded Green's function is antisymmetric in the Cartesian indices, only diagonal elements make a contribution to the pinning force. The diagonal elements of the free retarded Green's function are identical, $D_{t0}^{Rxx}=D_{t0}^{Ryy}$, and given by

$$D_{t0}^{Rxx}=\theta(t)\frac{-\eta}{\eta^2+\alpha^2}\left[1+\left(\frac{\alpha}{\eta}\sin\frac{\alpha t}{m}-\cos\frac{\alpha t}{m}\right)e^{-\eta t/m}\right], \tag{90}$$

and we obtain for the pinning force, for vanishing mass $m \ll \eta^2 r_p^3/\sqrt{\nu_0}$,

$$\mathbf{F}_p=-\frac{\eta\nu_0}{4\pi(\eta^2+\alpha^2)r_p^4 v^2}\mathbf{v}. \tag{91}$$

We observe that the pinning force is suppressed by the Hall force in the high-velocity limit $v \gg \sqrt{\nu_0}(\eta^2+\alpha^2)^{-1/2}r_p^{-2}$, and the high-velocity regime therefore sets in at a lower value in the presence of the Hall force.

At high temperatures $T \gg \sqrt{\nu_0}/r_p$ and moderate velocities $v < \eta\sqrt{\nu_0}/[(\eta^2+\alpha^2)r_p^2]$, the Hall force has the opposite effect; i.e., it increases the pinning force, as a calculation similar to the one leading to Eq. (80) shows that the pinning force is ($m \ll \eta^2 r_p^3/\sqrt{\nu_0}$)

$$\mathbf{F}_p=-\frac{\nu_0(\eta^2+\alpha^2)}{8\pi\eta T^2 r_p^2}\mathbf{v}. \tag{92}$$

We have found by solving the self-consistent equations numerically at high temperature $T=10\sqrt{\nu_0}/r_p$ that the pinning force is linear at low velocities and increases with increasing Hall force. The deviation from linear behavior in the presence of the Hall force starts at a lower velocity value in accordance with the high-velocity regime starting at a lower value in the presence of the Hall force.

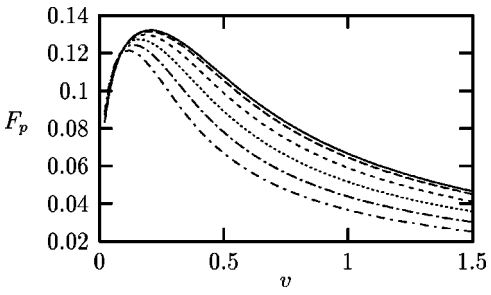

FIG. 7. Pinning force (in units of $\nu_0^{1/2}r_p^{-2}$) on a single vortex as a function of velocity (in units of $\eta^{-1}r_p^{-2}\nu_0^{1/2}$) obtained from the self-consistent theory for various strengths of the Hall force. The different curves correspond to $\alpha/\eta=0,0.2,0.4,0.6,0.8,1$, where the uppermost curve corresponds to $\alpha=0$ ($m=0.1\eta^2 r_p^3\nu_0^{-1/2}$ and $T=0.1\nu_0^{1/2}r_p^{-1}$).

2. Numerical results

For any given average velocity of the vortex, the pinning force can be calculated from the self-consistent theory. We have numerically calculated the pinning force for various strengths of the Hall force. In Fig. 7, the resulting pinning

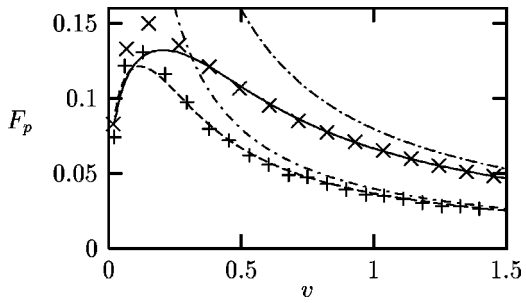

FIG. 8. Pinning force (in units of $10^{-4}\nu_0^{1/2}r_p^{-2}$) on a single vortex as a function of velocity. Comparison of the simulation results and the results of the self-consistent and lowest-order perturbation theory, Eq. (91), for the case of no Hall force, $\alpha=0$, and a moderately strong Hall force, $\alpha=\eta$ ($m=0.1\eta^2r_p^3\nu_0^{-1/2}$ and $T=0.1\nu_0^{1/2}r_p^{-1}$). The solid line represents the self-consistent result and the crosses the simulation result, while the upper dash-dotted line represents the perturbation theory result, all for the case $\alpha=0$. The dashed line and the plus symbols represent the self-consistent and simulation results, while the lower dash-dotted line represents the perturbation theory result, all for the case $\alpha=\eta$.

force as a function of the velocity is shown for different strengths of the Hall force for a temperature lower than the average barrier height, $T<\sqrt{\nu_0}/r_p$. The Hall force is seen to reduce the pinning force in this temperature regime except, of course, at low velocities.

In Fig. 8 we compare the pinning force obtained from the self-consistent theory with the result of perturbation theory valid at high velocities, Eq. (91), and simulations. According to Fig. 8, the reduction of the pinning force due to the Hall force predicted by the self-consistent and the perturbation theory is in good agreement at high velocities. The pinning forces obtained from the self-consistent theory and the simulations are also in good agreement in the presence of a Hall force, even at lower velocities, in fact in much better agreement than in the absence of the Hall force, in accordance with the fact that the Hall force suppresses the velocity fluctuations, as we demonstrate shortly.

The Hall angle calculated from the self-consistent theory approaches from below the disorder-independent value $\arctan(\alpha/\eta)$ at high velocities, as shown in Fig. 9. In Fig. 9, the Hall angle obtained from the self-consistent theory is also

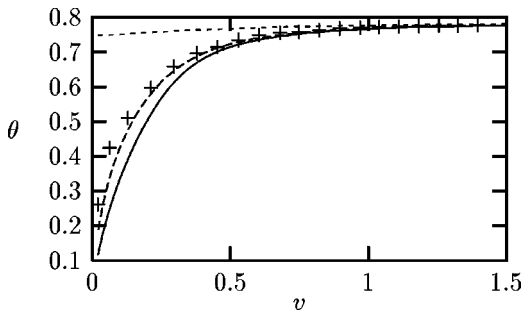

FIG. 9. Hall angle as a function of velocity for a single vortex. The curves represent the self-consistent results for the three temperatures $T=0,0.1,1$ (in units of $\nu_0^{1/2}r_p^{-1}$), where the uppermost curve corresponds to the highest temperature. The plus symbols represent the simulation results for the temperature $T=0.1\nu_0^{1/2}r_p^{-1}$. The parameter α/η is one and $m=0.1\eta^2r_p^3\nu_0{}^{1/2}$.

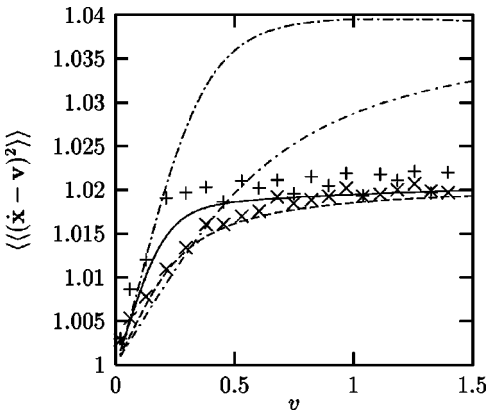

FIG. 10. Dependence of the single vortex velocity fluctuations (in units of $\eta^{-2}r_p^{-4}\nu_0$) on the average velocity (in units of $\eta^{-1}r_p^{-2}\nu_0^{1/2}$) for $\alpha=\eta$ and $\alpha=0$ ($T=0.1\nu_0^{1/2}/r_p$ and $m=0.1\eta^2r_p^3\nu_0^{-1/2}$). The solid and dashed lines represent the longitudinal and transverse velocity fluctuations, respectively, calculated using the self-consistent theory for the case $\alpha=\eta$, and the plus symbols and crosses represent the corresponding simulation results. The two dash-dotted lines represent the longitudinal and transverse velocity fluctuations, respectively, calculated using the self-consistent theory in the absence of the Hall force, $\alpha=0$, which were compared to simulations in Fig. 6.

compared to simulations, and the agreement is seen to be good. As apparent from Fig. 9, an increase in the temperature increases the Hall angle at low velocities, because the effective friction coefficient decreases with increasing temperature, and this feature vanishes at high velocities. From Fig. 9 we can also infer the following behavior of the Hall angle at zero velocity: At low temperatures it is zero, since the dependence of the pinning force at low velocities is sublinear. At a certain temperature, the Hall angle at zero velocity jumps to a finite value, since the pinning force then depends linearly on the velocity, and saturates at high temperatures at the disorder independent value.

We have also determined the influence of the Hall force on the velocity fluctuations as shown in Fig. 10. We observe that the Hall force at low velocities slightly increases the transverse velocity fluctuations, and decreases the longitudinal fluctuations, whereas the longitudinal and transverse velocity fluctuations are strongly suppressed by the Hall force at higher velocities, in particular the longitudinal fluctuations. The suppression of the velocity fluctuations is due to the blurring by the Hall force of the preferred direction of motion due to the external force, resulting in a less jerky motion. At high average velocity, the longitudinal and transverse velocity fluctuations saturate and become equal because of the strong friction. As previously discussed in the absence of the Hall force, the saturation value can be determined from the energy conservation relation [which takes the same form, Eq. (85), as in the absence of the Hall force, since the Hall force does not perform any work] and the high-velocity expression for the pinning force, Eq. (91), since our numerical results show that the second term on the left side of Eq. (84) is independent of the Hall force and velocity (and disorder). This observation tells us that the suppression of the velocity fluctuations caused by the Hall force, according to the energy conservation relation, Eq. (84), is in correspondence with the suppression of the pinning force.

We note from Fig. 10 that the high-velocity regime sets in at lower velocities than in the absence of the Hall force. In Fig. 10, the velocity fluctuations calculated using the self-consistent theory are also compared to simulations, and the agreement is seen to be good.

We have ascertained the convergence of the numerical iteration process by testing that the obtained solutions satisfy the energy conservation relation. We find that the energy conservation relation is fulfilled within an accuracy of 2%, except at the lowest velocities.

V. VORTEX LATTICE

After having gained confidence in the Hartree approximation studying the case of a single vortex, we consider in this section the influence of pinning on a vortex lattice in the flux flow regime, where the lattice moves with a constant average velocity $\langle\langle \dot{\mathbf{u}}_{\mathbf{R}t} \rangle\rangle = \mathbf{v}$, since the external force is assumed independent of time. We consider a triangular Abrikosov vortex lattice, and treat the interaction between the vortices in the harmonic approximation. The free retarded Green's function of the vortex lattice

$$D^R_{\mathbf{q}\omega} = \sum_b \frac{\mathbf{e}_b(\mathbf{q})\mathbf{e}_b(\mathbf{q})}{m\omega^2 + i\eta\omega - K_b(\mathbf{q})} \tag{93}$$

is obtained by diagonalizing the dynamic matrix, and inverting the inverse free retarded Green's function specified by Eq. (14) (for the moment we neglect the Hall force). The sum in Eq. (93) is over the two modes, $b=1,2$, corresponding to eigenvectors $\mathbf{e}_b(\mathbf{q})$ and eigenvalues $K_b(\mathbf{q})$, respectively. The eigenvalues and eigenvectors of the dynamic matrix are periodic with respect to translations by reciprocal lattice vectors.

Since the lattice distortions of interest are of small wavelength compared to the lattice constant, the dynamic matrix of the vortex lattice is specified by the continuum theory of elastic media, i.e., through the compression modulus c_{11} and the shear modulus c_{66} according to[18]

$$\Phi_{\mathbf{q}} = \frac{\phi_0}{B} \begin{pmatrix} c_{11}q_x^2 + c_{66}q_y^2 & (c_{11}-c_{66})q_xq_y \\ (c_{11}-c_{66})q_xq_y & c_{66}q_x^2 + c_{11}q_y^2 \end{pmatrix}, \tag{94}$$

where $\mathbf{q}$ belongs to the first Brillouin zone, B is the magnitude of the external magnetic field, and ϕ_0/B is therefore equal to the area a^2 of the unit cell of the vortex lattice. In the continuum limit we obtain a longitudinal branch $\mathbf{e}_l(\mathbf{q})\cdot\hat{\mathbf{q}}=1$, with corresponding eigenvalues $K_l(\mathbf{q}) = c_{11}a^2q^2$, and a transverse branch $\mathbf{e}_t(\mathbf{q})\cdot\hat{\mathbf{q}}=0$, with corresponding eigenvalues $K_t(\mathbf{q}) = c_{66}a^2q^2$.

A. High-velocity limit

At high velocities $v \gg \sqrt{\nu_0}/(\eta r_p^2)$, where lowest-order perturbation theory in the disorder is valid, we can neglect the self-energies in the self-consistent expression for the pinning force, Eq. (64); i.e., we can insert the free retarded Green's function for the lattice and, assuming $v \gg T/(\eta r_p)$, neglect the fluctuation exponent, and obtain for the pinning force

$$\mathbf{F}_p = -\int \frac{d\mathbf{k}}{(2\pi)^2}\mathbf{k}\nu(\mathbf{k}) \sum_{b=l,t} \frac{\eta\mathbf{k}\cdot\mathbf{v}[\mathbf{k}\cdot\mathbf{e}_b(\mathbf{k})]^2}{(\eta\mathbf{k}\cdot\mathbf{v})^2 + [K_b(\mathbf{k})]^2}. \tag{95}$$

The maximum values, attained at the boundaries of the Brillouin zones, of the transverse and longitudinal eigenvalues are specified by the compression and shear moduli $K_t \sim c_{66}$ and $K_l \sim c_{11}$. The compression modulus is much greater than the shear modulus, $c_{11} \gg c_{66}$, in thin films and high-temperature superconductors.[19] The order of magnitude of the first term in the denominator of Eq. (95) is $\eta v^2 r_p^{-2}$, since the range of the impurity correlator is r_p, and at intermediate velocities $c_{66}r_p/\eta \ll v \ll c_{11}r_p/\eta$, only the transverse mode therefore contributes to the pinning force, and we obtain

$$\mathbf{F}_p = -\int \frac{d\mathbf{k}}{(2\pi)^2}\mathbf{k}\nu(\mathbf{k}) \frac{[\mathbf{k}\cdot\mathbf{e}_t(\mathbf{k})]^2}{\eta\mathbf{k}\cdot\mathbf{v}}. \tag{96}$$

The eigenvalues $\mathbf{e}_t(\mathbf{k})$ are periodic in reciprocal lattice, and assuming short-range disorder $r_p \ll a$, the rest of the integrand is slowly varying, and we obtain for the pinning force

$$\mathbf{F}_p = -\frac{1}{2}\int \frac{d\mathbf{k}}{(2\pi)^2}\mathbf{k}\frac{\nu(\mathbf{k})k^2}{\eta\mathbf{k}\cdot\mathbf{v}} = -\frac{\nu_0}{8\pi r_p^4 \eta v^2}\mathbf{v}. \tag{97}$$

At very high velocities $v \gg c_{11}r_p/\eta$, the eigenvalues of the dynamic matrix in Eq. (95) can be neglected compared to the velocity-dependent term in the denominator, and the longitudinal and transverse parts of the free retarded Green's function give equal contributions to the pinning force, and we obtain

$$\mathbf{F}_p = -\frac{\nu_0}{4\pi r_p^4 \eta v^2}\mathbf{v}. \tag{98}$$

This result is identical to the expression for the pinning force on a single vortex, Eq. (70), in the high-velocity regime $v \gg \sqrt{\nu_0}/(\eta r_p^2)$, since the influence of the elastic interaction is negligible.

B. Numerical results

In this section we consider the pinning force on the vortex lattice obtained from the self-consistent theory. For any given average velocity of the lattice, the coupled equations of Green's functions and self-energies, Eq. (55) and Eq. (56), may be solved numerically by iteration. In order to simplify the numerical calculation, the self-consistent equations are brought to dimensionless form by introducing the following units for length, time, and mass: a, $\eta a^3/\nu_0^{1/2}$, and $\eta^2 a^4/\nu_0^{1/2}$. Starting by neglecting the self-energies, we obtain numerically the response and correlation functions. From Eq. (64) we can then determine the pinning force as a function of the velocity. We have calculated the velocity dependence of the pinning force for vortex lattices of sizes 4×4, 8×8, and 16×16 using the self-consistent theory, and the results are shown in Fig. 11. The difference between the results obtained for the 8×8 and the 16×16 lattice is small, and we conclude that the pinning force is fairly insensitive to the size of the lattice.

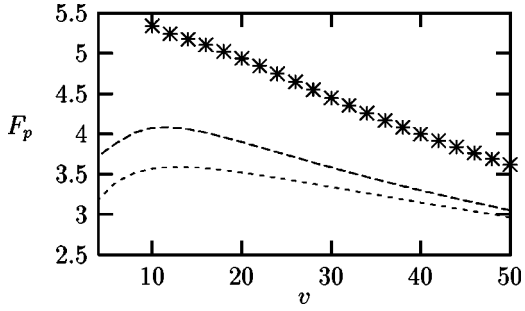

FIG. 11. Pinning force (in units of $\nu_0^{1/2}a^{-2}$) as a function of velocity (in units of $\eta^{-1}\nu_0^{1/2}a^{-2}$) obtained from the self-consistent theory for three different lattice sizes. The stars correspond to a 4×4 lattice, and the two curves correspond to 8×8 and 16×16 lattices, respectively. The mass and temperature are chosen to be zero, the elastic constants are given by $c_{66}a^3=100\nu_0^{1/2}$ and $c_{11}a^3=10^4\nu_0^{1/2}$, and the range of the disorder correlator is chosen to be $r_p=0.1a$.

In Fig. 12 we compare the pinning force as a function of the velocity for lattices of different stiffnesses, and we find that the pinning force decreases with increasing stiffness of the lattice. Generally, the interaction between the vortices lowers the pinning force, since the neighboring vortices in a moving lattice drag a vortex over the potential barriers. This can be inferred from the self-consistent theory by comparing the pinning forces depicted in Figs. 2 and 14, and in perturbation theory by noting the extra term originating from the elastic interaction in the denominator of the expression for the pinning force, Eq. (95).

When the temperature is increased, the pinning force decreases, except at very high velocity, as apparent from Fig. 13. This feature is common to the single-vortex case, and simply reflects that thermal noise helps a vortex over the potential barriers.

The convergence of the iterative procedure is monitored by checking that energy conservation is fulfilled. The energy conservation relation for a vortex lattice is obtained as in Sec. IV E 2, and since the term originating from the harmonic interaction between the vortices disappears due to the symmetry property of the dynamic matrix, Eq. (5), we obtain for a vortex lattice the energy conservation relation

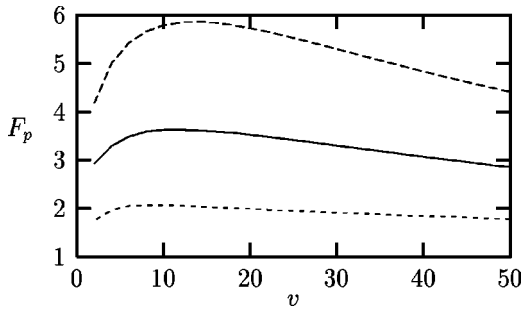

FIG. 12. Pinning force (in units of $\nu_0^{1/2}a^{-2}$) on a vortex lattice of size 16×16 as a function of velocity (in units of $\eta^{-1}\nu_0^{1/2}a^{-2}$) obtained from the self-consistent theory for the compression modulus given by $c_{11}a^3=10^4\nu_0^{1/2}$ and three different shear moduli: $c_{66}a^3=50\nu_0^{1/2}$ (upper dashed line), $c_{66}a^3=100\nu_0^{1/2}$ (solid line), and $c_{66}a^3=200\nu_0^{1/2}$ (lower dashed line). The mass and temperature are both chosen to be zero, and $r_p=0.1a$.

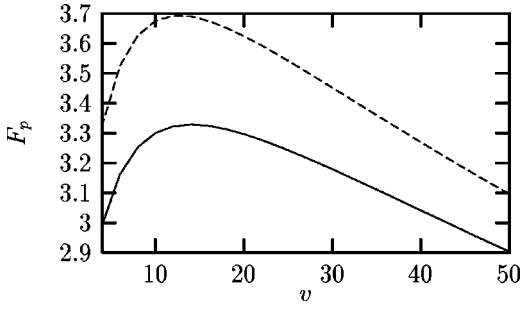

FIG. 13. Pinning force (in units of $\nu_0^{1/2}a^{-2}$) on a vortex lattice of size 16×16 as a function of velocity (in units of $\eta^{-1}\nu_0^{1/2}a^{-2}$) obtained from the self-consistent theory for two different temperatures. The elastic constants are given by $c_{66}a^3=100\nu_0^{1/2}$ and $c_{11}a^3=10^4\nu_0^{1/2}$, and $r_p=0.1a$, and $m=1.0\times10^{-4}\eta^2a^3\nu_0^{-1/2}$. The dashed line corresponds to $T=0$, and the solid line to $T=0.5\nu_0^{1/2}a^{-1}$.

$$\eta\partial_t \,\mathrm{tr}[-i\partial_t G^K(\mathbf{R},t;\mathbf{R},t')+2TG^R(\mathbf{R},t;\mathbf{R},t')]|_{t'=t} = -\mathbf{v}\cdot\mathbf{F}_p\,. \tag{99}$$

The convergence of the iteration procedure, employed when solving the self-consistent equations, has been checked by numerically calculating the terms in Eq. (99). We find that the right and left sides of the energy conservation relation differ by no more than a few percent after 20 iterations.

C. Hall force

We now consider the influence of a Hall force on the dynamics of a vortex lattice. The motion of the vortex lattice, with its associated magnetic field, induces an average electric field. The relationship between the average vortex velocity and the induced electric field, $\mathbf{E}=\mathbf{v}\times\mathbf{B}$, and the expression for the Lorentz force, yields for the resistivity tensor of a superconducting film

$$\rho=\frac{\phi_0 B}{\eta_{\mathrm{eff}}^2+\alpha^2}\begin{pmatrix}\eta_{\mathrm{eff}} & \alpha\\ -\alpha & \eta_{\mathrm{eff}}\end{pmatrix}, \tag{100}$$

where the effective friction coefficient η_{eff} was introduced in Eq. (8), and has previously only been determined to lowest order in the disorder.[17] According to Eq. (100), the following relationship between the transverse, ρ_{xy}, and the longitudinal resistivities, ρ_{xx}, is obtained:

$$\rho_{xy}=\rho_{xx}^2\frac{\alpha}{B\phi_0}\left(1+\frac{\alpha^2}{\eta_{\mathrm{eff}}^2}\right). \tag{101}$$

If the Hall force is small, $\alpha\ll\eta_{\mathrm{eff}}$, the scaling law[12]

$$\rho_{xy}=\rho_{xx}^2\frac{\alpha}{B\phi_0} \tag{102}$$

is seen to be obeyed. This scaling law is valid for all velocities of the vortex, provided the Hall force is small compared to the friction force, $\alpha\ll\eta$. We note that the scaling law is also valid at small vortex velocities for arbitrary values of the Hall force, if the effective friction coefficient diverges at small velocities. This occurs if the pinning force decreases slower than linearly in the vortex velocity. This is indeed the

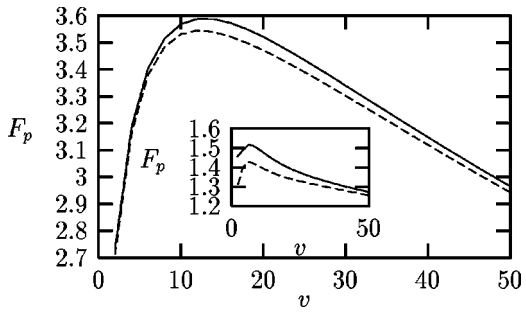

FIG. 14. Pinning force (in units of $\nu_0^{1/2}a^{-2}$) on a vortex lattice of size 16×16 as a function of velocity (in units of $\eta^{-1}\nu_0^{1/2}a^{-2}$) obtained from the self-consistent theory. The solid and dashed lines correspond to $\alpha=0$ and $\alpha=\eta$, respectively. The temperature and mass are both chosen to be zero, and $r_p=0.1a$. The elastic constants are given by $c_{11}a^3=10^4\nu_0^{1/2}$ and $c_{66}a^3=100\nu_0^{1/2}$. Inset: pinning force as a function of velocity for $\alpha=0$ and $\alpha=\eta$, respectively. Here $c_{66}a^3=300\nu_0^{1/2}$ and the other parameters are unchanged.

case, according to the self-consistent theory, at temperatures lower than the average barrier height, $T\ll\sqrt{\nu_0}/r_p$, as indicated by the low-velocity behavior of the pinning force in Fig. 14. This behavior of the pinning force is also obtained for noninteracting vortices as apparent from Fig. 7.

In Fig. 14 is shown the pinning force obtained from the self-consistent theory as a function of velocity for the case of zero temperature. As expected there is no influence of the Hall force on the pinning force at low velocities, but we find a suppression at intermediate velocities, and at very high velocities $v\gg c_{11}a/\eta$ we recover the high-velocity limit of the single vortex result, i.e., Eq. (91). By comparison of Figs. 7 and 14, we find that the Hall force has a much weaker influence at intermediate velocities on the pinning of an interacting vortex lattice than on a system of noninteracting vortices. Furthermore, the influence of the Hall force on the pinning force is more pronounced for a stiff than a soft lattice as seen from the inset in Fig. 14. In Fig. 15 the dependence of the Hall angle on the velocity is presented for various stiffnesses of the vortex lattice; the stiffest lattice has the greatest Hall angle. Since the pinning force is reduced by the interaction between the vortices, the Hall angle for a lattice is

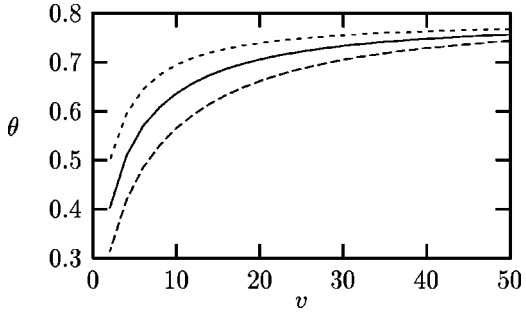

FIG. 15. Hall angle obtained from the self-consistent theory for a vortex lattice of size 16×16 as a function of velocity (in units of $\eta^{-1}\nu_0^{1/2}a^{-1}$) for a moderately strong Hall force, $\alpha=\eta$. The compression modulus is given by $c_{11}a^3=10^4\nu_0^{1/2}$, and the three curves correspond to decreasing values of the shear modulus: $c_{66}a^3=200\nu_0^{1/2}$, $100\nu_0^{1/2}$, and $50\nu_0^{1/2}$. The mass and temperature are both chosen to be zero, and $r_p=0.1a$.

larger than for an independent vortex, except at high velocities where they saturate at the same value. A similar behavior of the Hall angle at zero velocity as observed for a single vortex in Sec. IV E 2 pertains to a vortex lattice.

VI. DYNAMIC MELTING

In this section we consider the influence of quenched disorder on the dynamic melting of a vortex lattice. This nonequilibrium phase transition has been studied experimentally[4] as well as through numerical simulation and a phenomenological theory and perturbation theory.[6,20,21] The notion of dynamic melting refers to the melting of a moving vortex lattice where in addition to the thermal fluctuations, fluctuations in vortex positions are induced by the disorder. A temperature-dependent critical velocity distinguishes a transition between a phase where the vortices form a moving lattice, the solid phase, and a vortex liquid phase.

Before solving the self-consistent equations by numerical iteration in order to obtain the phase diagram, we consider the heuristic argument for determining the phase diagram for dynamic melting of a vortex lattice presented in Ref. 6. There, the disorder-induced fluctuations were estimated by considering the correlation function

$$\kappa_{\alpha\alpha'}(\mathbf{x},t)=\langle\langle f_\alpha^{(p)}(\mathbf{x},t)f_{\alpha'}^{(p)}(\mathbf{0},0)\rangle\rangle \tag{103}$$

of the pinning force density

$$\mathbf{f}^{(p)}(\mathbf{x},t)=-\sum_{\mathbf{R}}\delta(\mathbf{x}-\mathbf{R}-\mathbf{u}_{\mathbf{R}t})\nabla V(\mathbf{x}-\mathbf{v}t). \tag{104}$$

Neglecting the interdependence of the fluctuations of the vortex positions and the fluctuations in the disorder potential, the pinning force correlation function factorizes:

$$\kappa_{\alpha\alpha'}(\mathbf{x},t)\simeq\sum_{\mathbf{R}\mathbf{R}'}\langle\langle\delta(\mathbf{x}-\mathbf{R}-\mathbf{u}_{\mathbf{R}t})\delta(\mathbf{R}'-\mathbf{u}_{\mathbf{R}'0})\rangle\rangle \times\nabla_\alpha\nabla_{\alpha'}\langle\langle V(\mathbf{x}-\mathbf{v}t)V(\mathbf{0})\rangle\rangle. \tag{105}$$

Introducing the Fourier transform (A is the area of the film)

$$C_{\mathbf{R}\mathbf{R}'}(\mathbf{q},t)=A^{-1}\langle\langle e^{-i\mathbf{q}\cdot(\mathbf{R}+\mathbf{u}_{\mathbf{R}t}-\mathbf{R}'-\mathbf{u}_{\mathbf{R}'0})}\rangle\rangle \tag{106}$$

of the vortex density-density correlation function

$$C_{\mathbf{R}\mathbf{R}'}(\mathbf{x},t)=\langle\langle\delta(\mathbf{x}-\mathbf{R}-\mathbf{u}_{\mathbf{R}t})\delta(\mathbf{R}'-\mathbf{u}_{\mathbf{R}'0})\rangle\rangle, \tag{107}$$

and employing the translational invariance yields

$$\kappa_{\alpha\alpha'}(\mathbf{x},t)=-n_V\sum_{\mathbf{R}\mathbf{R}'}\langle\langle\delta(\mathbf{x}-\mathbf{R}-\mathbf{u}_{\mathbf{R}t}-\mathbf{R}'-\mathbf{u}_{\mathbf{R}'0})\rangle\rangle \times\nabla_\alpha\nabla_{\alpha'}\nu(\mathbf{x}-\mathbf{v}t), \tag{108}$$

where n_V is the density of vortices. In the fluidlike phase the motion of different vortices is ''incoherent'' and the off-diagonal terms $\mathbf{R}\neq\mathbf{R}'$ can be neglected, yielding

$$\kappa_{\alpha\alpha'}(\mathbf{x},t)=-n_V\delta(\mathbf{x})\nabla_\alpha\nabla_{\alpha'}\nu(\mathbf{v}t). \tag{109}$$

In analogy with the noise correlator, the effect of disorder-induced fluctuations is then represented by a ''shaking temperature''

$$T_{\mathrm{sh}}=\frac{1}{4\eta n_V}\sum_{\alpha}\int d\mathbf{x}\int_{-\infty}^{\infty}dt\,\kappa_{\alpha\alpha}(\mathbf{x},t)=\frac{1}{4\sqrt{2\pi}}\frac{\nu_0}{\eta v r_p^3}$$

$$=\frac{1}{4\sqrt{2\pi}}\frac{\nu_0}{F r_p^3}, \tag{110}$$

where in the last equality it is assumed that the pinning force is small compared to the friction force, i.e., $\eta v \simeq F$. An effective temperature is then obtained by adding the ''shaking temperature'' to the temperature, $T_{\mathrm{eff}}=T+T_{\mathrm{sh}}$, and according to Eq. (110) the effective temperature decreases with increasing external force, i.e., with increasing average velocity of the vortices. As the external force is increased the fluid thus freezes into a lattice. The value of the external force for which the moving lattice melts, the transition force F_t, is in this ''shaking'' theory defined as the value for which the effective temperature equals the melting temperature T_m in the absence of disorder,

$$T_{\mathrm{eff}}(F=F_t)=T_m, \tag{111}$$

and has therefore in the shaking theory the temperature dependence

$$F_t(T)=\frac{\nu_0}{4\sqrt{2\pi}r_p^3(T_m-T)}, \tag{112}$$

for temperatures below the melting temperature of the ideal lattice. We note that the transition force for strong enough disorder exceeds the critical force for which the lattice is pinned $F_t > F_c \sim \nu_0^{1/2}/r_p^2$.

We now describe the calculation within the self-consistent theory of the physical quantities of interest for dynamic melting. The conventional way of determining a melting transition is to use the Lindemann criterion, which states that the lattice melts when the displacement fluctuations reach a critical value $\langle \mathbf{u}^2\rangle = c_L^2 a^2$, where c_L is the Lindemann parameter, which is typically in the interval ranging from 0.1 to 0.2, and a^2 is the area of the unit cell of the vortex lattice. In two dimensions the position fluctuations of a vortex diverge even for a clean system, and the Lindemann criterion implies that a two-dimensional vortex lattice is always unstable against thermal fluctuations. However, a quasi-long-range translational order persists up to a certain melting temperature.[20] As a criterion for the loss of long-range translational order a modified Lindemann criterion involving the relative vortex fluctuations

$$\langle [\mathbf{u}(\mathbf{R}+\mathbf{a}_0,t)-\mathbf{u}(\mathbf{R},t)]^2\rangle = 2c_L^2 a^2, \tag{113}$$

where $\mathbf{a}_0$ is a primitive lattice vector, has successfully been employed,[20] and its validity verified within a variational treatment.[22] The relative displacement fluctuations of the vortices are specified in terms of the correlation function according to

$$\langle\langle [\mathbf{u}(\mathbf{R}+\mathbf{a}_0,t)-\mathbf{u}(\mathbf{R},t)]^2\rangle\rangle = 2i\,\mathrm{tr}[G^K(\mathbf{0},0)-G^K(\mathbf{a}_0,0)], \tag{114}$$

where the translation invariance of the Green's functions has been exploited. The correlation function is determined by the Dyson equation, Eq. (73), where the influence of the quenched disorder appears explicitly through Σ^K and implicitly through Σ^R and Σ^A in the retarded and advanced response functions. Furthermore, the self-energies depend self-consistently on the response and correlation functions. We have calculated numerically the Green's functions and self-energies and thereby the vortex fluctuations for a vortex lattice of size 8×8, and evaluated the pinning force from Eq. (64).

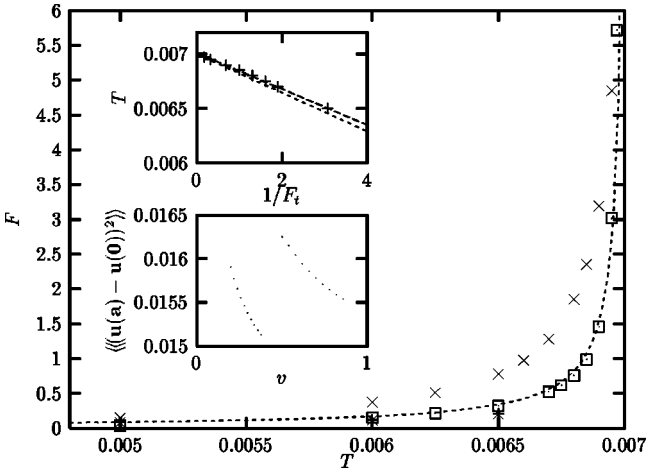

FIG. 16. Phase diagram for the dynamic melting transition. The melting curve separates the two phases—for values of the external force larger than the transition force the moving vortices form a solid and for smaller values a liquid. The dots in the boxes represent points on the melting curve obtained from the self-consistent theory using a vortex lattice of size 8×8, while the three stars represent the simulation results of Ref. 6. The crosses represent the lowest-order perturbation theory results. The dashed line is the curve $F_t(T)=1.77\times 10^{-4}/(0.007-T)$, the melting curve predicted by the shaking theory. Upper inset: relationship between temperature and the inverse transition force obtained from the self-consistent theory, close to the melting temperature, for the particular value of the Lindemann parameter $c_L=0.124$, for which the curve intersects the vertical axis at $T_m=0.00701$. The set of points calculated from the self-consistent theory (plus signs) coincides with a straight line in excellent agreement with the prediction for the critical exponent by the shaking theory being 1. Lower inset: relative displacement fluctuations as a function of velocity. The dots to the left are calculated using the self-consistent theory and the dots to the right using lowest-order perturbation theory (for the temperature $T=0.0065$).

We determine the phase diagram for dynamic melting of the vortex lattice by calculating the relative displacement fluctuations for a set of velocities, and interpolate to find the transition velocity v_t, i.e., the value of the velocity at which the fluctuations fulfill the modified Lindemann criterion (the determination of the Lindemann parameter is discussed shortly). An example of such a set of velocities is presented in the lower inset in Fig. 16, where the relative displacement fluctuations as a function of velocity are shown. The magnitude of the transition force is determined by the averaged equation of motion

$$F_t=\eta v_t + F_p(v_t) \tag{115}$$

and is then obtained by using the numerically calculated pinning force. Repeating the calculation of the transition force for various temperatures determines the melting curve, i.e.,

the temperature dependence of the transition force, $F_t(T)$, separating two phases in the FT plane: a high-velocity phase where the vortices form a moving solid when the external force exceeds the transition force, $F>F_t(T)$, and a liquid phase for forces less than the transition force.

In order to be able to compare the results of the self-consistent theory to the simulation results, we use the same parameters as input to the self-consistent theory as used in the literature.[6] There, the melting temperature in the absence of disorder is given by $T_m=0.007$ [the unit of energy per unit length is taken to be $2(\phi_0/4\pi\lambda)^2$] as obtained by simulations of clean systems,[23] and assumed equal to the Kosterlitz-Thouless temperature[24,25]

$$T_{\mathrm{KT}}=\frac{c_{66}a^2}{4\pi}. \tag{116}$$

The shear modulus is therefore determined to have the value $c_{66}=0.088$ (as a is taken as the unit of length). The range of the vortex interaction λ was approximately equal to the lattice spacing a_0, giving for the compression modulus[11]

$$c_{11}=\frac{16\pi\lambda^2 c_{66}}{a_0^2}\simeq 50c_{66}\simeq 4.4. \tag{117}$$

The range and strength of the disorder correlator in the simulations are in the chosen units $r_p=0.2$ and $\nu_0=1.42\times10^{-5}$, and since the simulations are done for an overdamped system, the vortex mass in the self-consistent theory should be set to zero.

As described above, our numerical results for the relative displacement fluctuations can be used to obtain the dynamic phase diagram once the Lindemann parameter is determined. In order to do so we calculate ''melting'' curves using the self-consistent theory for a set of different values of the Lindemann parameter. We find that these curves have the same shape, close to the melting temperature, as the melting curve obtained from the shaking theory, Eq. (112),

$$T=C_1-\frac{C_2}{F_t}. \tag{118}$$

The curve which intersects at the melting temperature $T_m=0.007$, the one depicted in the upper inset in Fig. 16, i.e., the one for which C_1 is closest to the value 0.007, is then chosen, determining the Lindemann parameter to be given by the value $c_L=0.124$.

Having determined the Lindemann parameter, we can determine the melting curve, and the corresponding phase diagram obtained from the self-consistent theory is shown in Fig. 16. The simulation results[6] are also presented, as well as the melting curve obtained from the shaking theory. We note the agreement of the simulation with the self-consistent theory, as well as with the shaking theory, although the simulation data are not in the large velocity regime and the shaking argument is therefore not *a priori* valid.

In view of the good agreement between the self-consistent theory, the shaking theory, and the simulation, and the fact that we only have one fitting parameter at our disposal, the melting temperature in the absence of disorder, it is of interest to recall that while the melting curve obtained from the shaking theory was based on an argument only valid in the liquid phase—i.e., freezing of the vortex liquid was considered—the melting curve we obtained from the self-consistent theory is calculated in the solid phase; i.e., we consider melting of the moving lattice. Furthermore, the melting of the vortex lattice was in the simulation indicated by an abrupt increase in the structural disorder,[6] yet another melting criterion, and the agreement of the self-consistent theory with the simulation data therefore further validates the use of the modified Lindemann criterion.

As apparent from the upper inset in Fig. 16, the critical exponent obtained from the self-consistent theory, 1.0, is in excellent agreement with the prediction of the shaking theory, where the critical exponent equals 1. Furthermore, we find that the self-consistent theory yields the value 1.65×10^{-4} for the magnitude of the slope C_2, which is in good agreement with the value, $\nu_0/(4\sqrt{2\pi}r_p^3)=1.77\times10^{-4}$, predicted by the shaking theory, represented by the lower dashed line. That the values are so close testifies to the appropriateness of characterizing the disorder induced fluctuations effectively by a temperature.

It is of interest to compare the melting curves obtained from the self-consistent theory and perturbation theory. Expanding the Keldysh component of the Dyson equation, Eq. (55), to lowest order in the disorder we obtain

$$G^{K(1)}_{\mathbf{q}\omega}=D^R_{\mathbf{q}\omega}(\Sigma^{K(1)}_{\mathbf{q}\omega}-2i\eta T)D^A_{\mathbf{q}\omega}-2i\eta k_B T D^R_{\mathbf{q}\omega}(\Sigma^{R(1)}_{\mathbf{q}\omega}D^R_{\mathbf{q}\omega}+D^A_{\mathbf{q}\omega}\Sigma^{A(1)}_{\mathbf{q}\omega})D^A_{\mathbf{q}\omega}, \tag{119}$$

where $\Sigma^{R(1)}$, $\Sigma^{A(1)}$, and $\Sigma^{K(1)}$ are the lowest-order approximations of the self-energies, i.e., calculated to first order in ν_0. The relative vortex displacement fluctuations, Eq. (114), can then be obtained in perturbation theory from Eq. (119). In Fig. 16 are shown the melting curve predicted by perturbation theory, i.e., where we for the transition velocity interpolation use the relative vortex fluctuations obtained from perturbation theory, an example of which is shown in the lower inset. As to be expected, the perturbation theory result is in good agreement with the self-consistent theory, and the shaking theory, at high velocities. However, we observe from Fig. 16 that the melting curve obtained from lowest-order perturbation theory deviates markedly at intermediate velocities from the prediction of the nonperturbative self-consistent theory, and thereby from the shaking theory, which is known to account well for the measured melting curve (see Hellerqvist *et al.*[4]).

The shaking theory is seen to be in remarkable good agreement with the self-consistent theory for the parameter values considered above. We have investigated whether this feature persists for stronger disorder. As apparent from Fig. 17, there is a more pronounced difference between the shaking theory and the self-consistent theory at stronger disorder. Whereas the deviation between the self-consistent and shaking theory for the previous parameter values typically is 5%, in the case of a fivefold stronger disorder $\nu_0=7.1\times10^{-5}$, it is more than 15%.

VII. CONCLUSION

We have studied the influence of pinning on vortex dynamics in the flux flow regime. A self-consistent theory for the vortex correlation and response functions was con-

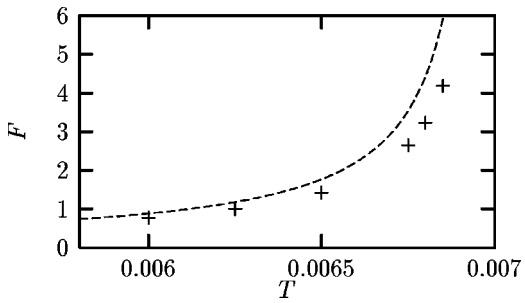

FIG. 17. Phase diagram for the dynamic melting transition for the disorder strength $\nu_0 = 7.1 \times 10^{-5}$. The plus signs represent points on the melting curve obtained from the self-consistent theory for a vortex lattice of size 8×8, while the dashed curve is the curve $F_t(T) = 8.85 \times 10^{-4}/(0.007 - T)$, the melting curve predicted by the shaking theory.

structed, allowing a nonperturbative treatment of the disorder. The validity of the self-consistent theory was established by comparison with numerical simulations of the Langevin equation.

The self-consistent theory was first applied to a single vortex, appropriate for low magnetic fields where the vortices are so widely separated that the interaction between them can be neglected. The result for the pinning force was compared to lowest-order perturbation theory and good agreement was found at high velocities, whereas perturbation theory failed to capture the nonmonotonic behavior at low velocities, a feature captured by the self-consistent theory. The influence of the Hall force on the pinning force on a single vortex was then considered using the self-consistent theory. The Hall force was observed to suppress the pinning force, an effect also confirmed by our simulations. The suppression of the pinning force was at high velocities shown to be in agreement with the analytical result obtained from lowest-order perturbation theory. The suppression of the pinning force was caused by the Hall force through its reduction of the response function, while the effect of fluctuations through the fluctuation exponent at not too high temperatures could be neglected. The situation at high temperatures was the opposite, since in that case the thermal fluctuations were of importance, and the Hall force then increased the pinning force because it suppressed the fluctuation exponent.

We also studied a vortex lattice treating the interaction between the vortices in the harmonic approximation. The pinning force on the vortex lattice was found to be reduced by the interaction. The pinning force as a function of velocity displayed a plateau at intermediate velocities, before eventually approaching at very high velocities the pinning force on a single vortex. Analytical results for the pinning force were obtained in different velocity regimes depending on the magnitude of the compression modulus of the vortex lattice. Furthermore, we included the Hall force and showed that its influence on the pinning force was much weaker on a vortex lattice than on a single vortex.

We developed a self-consistent theory of the dynamic melting transition of a vortex lattice, enabling us to determine numerically the melting curve directly from the dynamics of the vortices. The presented self-consistent theory corroborated the phase diagram obtained from the phenomenological shaking theory far better than lowest-order perturbation theory. The melting curve obtained from the self-consistent theory was found to be in good quantitative agreement with simulations and experimental data.

ACKNOWLEDGMENTS

It is a pleasure to acknowledge helpful discussions with Dr. Johannes Müllers. This work was supported by the Swedish Natural Research Council through Contract Nos. F-AA/FU 10199-314 (S.G.) and F-AA/FU 10199-313 (J.R.).

[1] V. M. Vinokur, M. V. Feigel'man, V. B. Geshkenbein, and A. I. Larkin, Phys. Rev. Lett. **65**, 259 (1990).

[2] D. Ertas and M. Kardar, Phys. Rev. Lett. **73**, 1703 (1994).

[3] J. M. Harris, N. P. Ong, R. Gagnon, and L. Taillefer, Phys. Rev. Lett. **74**, 3684 (1995).

[4] S. Bhattacharya and M. J. Higgins, Phys. Rev. Lett. **70**, 2617 (1993); W. K. Kwok, J. A. Fendrich, C. J. van der Beek, and G. W. Crabtree, *ibid.* **73**, 2614 (1994); U. Yaron, P. L. Gammel, D. A. Huse, R. N. Kleiman, C. S. Oglesby, E. Bucher, B. Batlogg, D. J. Bishop, K. Mortensen, and K. N. Clausen, Nature (London) **376**, 753 (1995); M. C. Hellerqvist, D. Ephron, W. R. White, M. R. Beasley, and A. Kapitulnik, Phys. Rev. Lett. **76**, 4022 (1996); M. J. Higgins and S. Bhattacharya, Physica C **257**, 232 (1996); M. Marchevsky, J. Aarts, P. H. Kes, and M. V. Indenbom, Phys. Rev. Lett. **78**, 531 (1997).

[5] M. C. Faleski, M. C. Marchetti, and A. A. Middleton, Phys. Rev. B **54**, 12 427 (1996); S. Ryu, M. Hellerqvist, S. Doniach, A. Kapitulnik, and D. Stroud, Phys. Rev. Lett. **77**, 5114 (1996); S. Spencer and H. J. Jensen, Phys. Rev. B **55**, 8473 (1997); K. Moon, R. T. Scallettar, and G. T. Zimányi, Phys. Rev. Lett. **77**, 2778 (1996).

[6] A. E. Koshelev and V. M. Vinokur, Phys. Rev. Lett. **73**, 3580 (1994).

[7] A. Schmid and W. Hauger, J. Low Temp. Phys. **11**, 667 (1973).

[8] A. L. Larkin and Yu. N. Ovchinnikov, Zh. Éksp. Teor. Fiz. **65**, 1704 (1973) [Sov. Phys. JETP **38**, 854 (1974)].

[9] J. Müller and A. Schmid, Phys. Rev. Lett. **75**, 136 (1995); Ann. Phys. (Leipzig) **4**, 757 (1995); J. Müllers, Ph.D. thesis, Universität Karlsruhe, 1995.

[10] J. M. Cornwall, R. Jackiw, and E. Tomboulis, Phys. Rev. D **10**, 2428 (1974).

[11] G. Blatter, M. V. Feigel'man, V. B. Geshkenbein, A. I. Larkin, and V. M. Vinokur, Rev. Mod. Phys. **66**, 1125 (1994).

[12] V. M. Vinokur, V. B. Geshkenbein, M. V. Feigel'man, and G. Blatter, Phys. Rev. Lett. **71**, 1242 (1993).

[13] H. K. Janssen, Z. Phys. B **23**, 377 (1976); R. Bausch, H. K. Janssen, and H. Wagner, *ibid.* **24**, 113 (1976); C. De Dominicis, Phys. Rev. B **18**, 4913 (1978); P. C. Martin, E. D. Siggia, and H. A. Rose, Phys. Rev. A **8**, 423 (1973).

[14] A. Schmid, J. Low Temp. Phys. **49**, 609 (1982); U. Eckern, W. Lehr, A. Menzel-Dorwarth, F. Pelzer, and A. Schmid, J. Stat. Phys. **59**, 885 (1990).

[15] J. Schwinger, J. Math. Phys. **2**, 407 (1961); L. V. Keldysh, Zh. Éksp. Teor. Fiz. **47**, 1515 (1964) [Sov. Phys. JETP **20**, 1018 (1965)].
[16] C. R. Werner and U. Eckern, Ann. Phys. (Leipzig) **6**, 595 (1997).
[17] Wu Liu, T. W. Clinton, and C. J. Lobb, Phys. Rev. B **52**, 7482 (1995).
[18] E. H. Brandt, Rep. Prog. Phys. **58**, 1465 (1995).
[19] E. H. Brandt, Int. J. Mod. Phys. B **5**, 751 (1999).
[20] S. Scheidl and V. M. Vinokur, Phys. Rev. B **57**, 13 800 (1998).
[21] S. Scheidl and V. M. Vinokur, Phys. Rev. E **57**, 2574 (1998).
[22] J. Kierfeld, T. Nattermann, and T. Hwa, Phys. Rev. B **55**, 626 (1997).
[23] J. M. Caillol, D. Levesque, J. J. Weis, and J. P. Hansen, J. Stat. Phys. **28**, 325 (1982).
[24] J. M. Kosterlitz and D. J. Thouless, J. Phys. C **6**, 1181 (1973).
[25] D. S. Fisher, Phys. Rev. B **22**, 1190 (1980).